Dan-Gheorghe Vrabie

ASPECTS OF MOLECULAR ORIENTATION AND RELAXATION OF A POLYSTYRENE HOMOPOLYMER, COPOLYMER AND BLEND

Mémoire présenté
à la Faculté des études supérieures de l'université Laval
dans le cadre du programme de maîtrise en Chimie
pour l'obtention du grade de maître ès sciences (M. Sc.)

Département de chimie
FACULTE DES SCIENCES ET DE GENIE
UNIVERSITE LAVAL
QUÉBEC

2007

Résumé

Diverses techniques peuvent être utilisées pour déterminer l'orientation moléculaire de matériaux polymères, comme par exemple la mesure du dichroïsme infrarouge à transformée de Fourier et de la biréfringence, qui fournissent des informations sur le second moment de la fonction d'orientation. L'orientation moléculaire d'un copolymère à base de polystyrène, poly(styrène-co-styrène acide sulfonique) 4.7% (PS-SSA 4.7%) et l'orientation moléculaire d'un mélange de PS-SSA 5.0% avec poly(styrène-co-4-vinyl pyridine) 4.5% (PS-VP 4.5%) sont comparées avec celle du polystyrène (PS). Pour le polystyrène, une vue plus globale du comportement de l'orientation est obtenue en utilisant le principe de superposition temps/température pour tracer une courbe maître d'orientation-relaxation pour des vitesses exponentielles d'étirage. Le modèle de Doi-Edwards est utilisé pour simuler les courbes d'orientation et de relaxation du PS et du PS-SSA4.7%.

Summary

For the measurement of molecular orientation, various techniques can be employed, for example Fourier Transform Infrared Dichroism and Birefringence that give information about the second moment of the orientation distribution function. The molecular orientation of a polystyrene (PS) based copolymer, poly(styrene-co-styrene sulphonic acid) 4.7% (PS-SSA 4.7%), and a blend of PS-SSA 5.0% with poly(styrene-co-4-vinyl pyridine) 4.5% (PS-VP 4.5%), is compared with that of polystyrene. For polystyrene, a more general view of the orientation behaviour is obtained by drawing a master orientation-relaxation curve for exponential velocities of stretching. The Doi-Edwards model is used to simulate the orientation and relaxation curves for polystyrene and for poly(styrene-co-styrene sulphonic acid) 4.7%.

Remerciements

À mes professeurs et directeurs de recherche, Madame C. Géraldine Bazuin et Monsieur Robert E. Prud'homme, je leur suis profondément reconnaissant de m'avoir accepté dans leurs équipes, d'avoir orienté ma recherche, de m'avoir encouragé et d'avoir consacré un temps précieux à des discussions très fructueuses. Qu'ils soient ici durablement remerciés.

De tout mon coeur j'aimerais remercier le professeur Denis Boudreau pour l'encouragement et ses conseils judicieux.

Je suis reconnaissant pour l'accueil chaleureux que m'a réservé Madame Rodica Plesu, aussi pour sa grande amabilité et disponibilité.

J'aimerais également exprimer mes remerciements à tous mes collègues, actuels et anciens avec qui j'ai vécu des moments mémorables.

Que tous mes amis et les personnes qui de près ou de loin m'ont entouré et conseillé tout au long du travail pour ce rapport, veuillent trouver ici l'expression de ma gratitude.

Je remercie ma famille qui m'a entouré toujours avec affection et joie.

Enfin, c'est à mon grand-père que je dédie ce travail.

Table of contents

LISTE OF TABLES

LIST OF FIGURES

1. Introduction

1.1. Literature Review

A large number of applications of polymeric materials depends on our understanding of their behaviour during mechanical deformation. In general terms, the deformation of polymer molecules and the relaxation of orientation of deformed polymers plays an important role in many processing methods. In addition, knowing the state of orientation permits a better control of the mechanical properties of the material. These processes are known to depend on many factors, including the molecular weights, the structure of the chain, etc. The molecular orientation of different homopolymers has been relatively well characterized (1).

Deformation mechanisms are more complex in the case of polymer blends in comparison to those of homopolymers. The analysis of the orientation mechanism of each component in a blend is of particular interest in understanding the relation between orientation and physical properties. Many studies of the orientation in polymer blends have been reported. Monnerie and coworkers studied the molecular orientation of miscible blends as polystyrene/poly (2,6-dimethyl 1,4,- phenylene oxide) (PS/PPO) (2-4) for temperatures above Tg, and observed that the orientation of the PS in the blend is higher than for pure PS. Also, they observed that the orientation of PPO is larger and remains constant over a broad range of composition. Studying the same system, Zhao and al. (5) explained this behaviour in terms of entanglement coupling, considering that PPO chains, diluted in a PS matrix, form more entanglements than do the PS chains with themselves.

For the polystyrene/poly(vinyl methyl ether) system (PS/PVME), it was observed that when PS/PVME films were stretched above their Tg the overall and individual orientations remain constant up to a critical concentration (6,7). Above this concentration it was observed that the orientation is composition dependent. This behaviour was explained in terms of a change of specific interactions between dissimilar chains with the blend composition.

For blends of poly(styrene-co-methacrylic acid) (PS-MAA) with poly(styrene-co-4-vinylpyridine) (PS-VP) that involve hydrogen bonding of the acid to pyridine, no increase was observed in the orientation as compared with that of PS (8). In comparison, the orientation of poly(styrene-co-styrene sulphonic acid) (PS-SSA) copolymers display an orientation that increases significantly when PS-SSA films are uniaxially stretched above their Tg. Due to strong hydrogen bonded ion-ion interactions that behave as effective crosslinks (9), an even greater enhancement in orientation was observed in blends of PS-SSA with PS-VP (10), where a proton transfer from the acid group to the pyridinium occurs. In Na-neutralized forms of PS-MAA and PS-SSA (ionomers), the microphase-separated domains called clusters have an important influence on the orientation behaviour, depending in particular on their relative proportion and their softening temperature range (11).

Theoretical models have been applied to the dynamics of amorphous homopolymers above their glass transition temperature, starting with the reptation model of de Gennes (12). In this theory, the chain moves by wriggling along its axis like a snake because a tubelike constraint, formed by the neighbouring macromolecules surrounding each chain, prohibits perpendicular motions. These tubelike constraints, or entanglements, develop from the interpenetration of random-coil chains (13) and are important in determining rheological, dynamic and fracture properties of the polymeric material.

The minor chain theory (14, 15) describes the orientation relaxation in terms of a single relaxation time through a reptation process. This time corresponds to the rearrangement of the chain conformation to about 70% of its initial value by a curvilinear diffusion along its contour.

In a more complex fashion, the Doi-Edwards model (DE) (16-19) describes the relaxation of the polymer chains by three relaxation processes. The first represents a local reequilibration and the corresponding relaxation time τ_A, is independent of molecular weight. The second relaxation process represents the retraction of the chain inside its tube, being characterized by a second relaxation time τ_B, which depends on the chain length, i.e. $\tau_B \sim M^2$. The terminal process is the slowest one where the chain recovers an isotropic configuration by reptation with a relaxation time $\tau_C \sim M^3$.

Various improvements have been proposed for the DE model. Viovy (20) considered that, at the end of the first relaxation process, the curvilinear monomer density is not the same on each side of the entanglement. Therefore, he proposed a new relaxation stage in which the monomers diffuse through entanglements in order to equilibrate the forces acting on each side. Another improvement was to take into account the chain length fluctuations (21) that can couple in the time scale of τ_B, with the retraction process. It was observed that chain length fluctuations can screen the retraction in practical situations. The DE model can also be corrected considering the concepts of tube relaxation (22), and of constraint release (23) or tube renewal (24) that arise from a self-consistent treatment of the relaxation of all the chains.

The effect of chain polydispersity was discussed in a stress relaxation analysis (18), showing that it can be significant even if the sample is nearly

monodisperse. In Ref. 14, the effect of polydispersity is discussed in terms of the minor chain theory, showing also that it influences to a great extent the orientation relaxation behaviour. The complexity of polydispersity effects on the orientation relaxation behaviour of polymeric materials motivated scientists to study model systems. For this reason, binary blends of well characterized nearly monodisperse, linear polymers of different molecular weights have been chosen as systems for investigation. It was observed that polydispersity can strongly retard the orientation relaxation of the low molecular weight component and decrease the longest relaxation time of the high molecular weight component (24). To explain this behaviour, it was considered that the orientation of the chain segments is influenced by an orientational coupling with the surroundings (25).

1.2. Theoretical Aspects of Orientation and Relaxation

1.2.1. Orientation Distribution and Orientation Averages

The orientation can be defined quantitatively. In Fig.1, a partially oriented polymer chain is shown, having its end-to-end separation vector denoted by R. This chain forms an angle θ with the reference axis z which is the deformation axis for the case of uniaxial orientation. Not all the chains are oriented similarly. It may be desirable to know the orientation of each chain but, since this is not an easy task, statistical aspects can be considered.

Figure 1:

Oriented chain showing preferential orientation along the reference axis z.
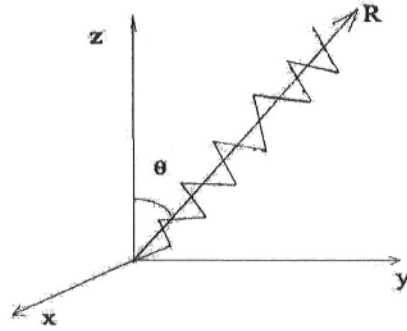
For a polymer chain subject to an uniaxial distribution of orientation in the drawing direction, a function f(θ) is defined so that f(θ)dθ represents the fraction of polymer chains whose axes lie within the small solid angle dθ at the angle θ to the draw direction such as:

$$2\pi \int_0^\pi f(\theta)\,\sin(\theta)\,d(\theta) = 1 \tag{1}$$

f(θ) can be expanded in terms of Legendre polynomials in cos θ as follows (26):

$$f(\theta) = \sum_l a_l P_l \cos(\theta) \tag{2}$$

If the assumption is made that the two opposite directions along the chain axis are equivalent, then f(θ) = f(π-θ) and a_n is zero unless n is even. The orthogonality of $P_l(\cos\theta)$ is then expressed by:

$$\int_0^\pi P_n(\cos\theta)\, P_m(\cos\theta)\,\sin\theta\,d\theta = 2/(2l+1) \times \delta_{mn} \tag{3}$$

5

where $\delta_{mn} = 0$ for $m \neq n$ and $\delta_{mn} = 1$ for $m = n$, and it follows that:

$$a_l = (1/2\pi)[(2l + 1)/2]\langle P_l(\cos\theta)\rangle \qquad (4)$$

where $\langle P_l(\cos\theta)\rangle$ is the value of $P_l(\cos\theta)$ averaged over the distribution. For $l = 0$, $\langle P_l(\cos\theta)\rangle = P_0(\cos\theta) = 1$; for a random distribution $\langle P_l(\cos\theta)\rangle = 0$ for all $l > 0$ whereas, for the case of a perfectly oriented sample, $\langle P_l(\cos\theta)\rangle = 1$ for all even l. $\langle P_l(\cos\theta)\rangle$ is expressed as a sum of terms in $\cos^n\theta$, with n even taking values from 2 to l. It can be written that:

$$\langle P_2(\cos\theta)\rangle = 1/2(3\cos^2\theta - 1) \qquad (5)$$

$$\langle P_4(\cos\theta)\rangle = (35\cos^4\theta - 30\cos^2\theta + 3)/8 \qquad (6)$$

and more generally:

$$\langle P_l(\cos\theta)\rangle = \int_0^\pi f(\theta)P_l(\cos\theta)\sin\theta\, d\theta \qquad (7)$$

where:

$$\langle\cos^l\theta\rangle = \int_0^\pi f(\theta)P_l(\cos^l\theta)\sin\theta\, d\theta \qquad (8)$$

Most of the methods for characterizing the molecular orientation give only limited information. It was shown (6) that, for an uniaxial distribution of molecular

orientations, the determination of $\langle P_2(\cos\theta)\rangle$ or $\langle P_4(\cos\theta)\rangle$ is sufficient in most cases (at not too high deformation ratios). Measurements of the infrared dichroism or refractive indices can give information about the second moment of the orientation distribution function only.

1.2.2. Infrared Dichroism

      The infrared spectrum of a compound provides important information about its chemical nature and molecular structure. Nearly all molecules absorb IR radiation, the exception being homonuclear diatomics. In order for a molecule to absorb radiation, there must be a change in dipole moment during the vibration. Each vibration is characterized by a transition moment M which has a certain orientation in the molecule. The intensity of the absorption band depends on the angle between the electric vector E of the incident radiation and the transition moment vector M. If a polymer sample is uniaxially stretched, the molecules tend to align in a specific direction. In other words, an optical anisotropy is induced, so the absorption of the sample is sensitive to the state of polarization of the incident radiation. If $A_{\parallel}$ and $A_{\perp}$ are the absorbancies of a given band measured with the radiation parallel and perpendicular, respectively, to the stretching direction, the ratio of these absorbancies is the dichroic ratio, R:

$$R = \frac{A_{\parallel}}{A_{\perp}} \tag{9}$$

The dichroic ratio is related to the second moment of the orientation distribution function P_2 by:

$$\langle P_2(\cos\theta)\rangle = 1/2\left(3\cos^2\theta - 1\right) = \left[(R-1)/(R+2)\right] \times \left[(R_0 + 2)/(R_0 - 1)\right] \qquad \textbf{(10)}$$

where $R_0 = 2\cot^2\alpha$, α being the angle between the transition moment associated with the considered absorption band and the main chain axis.

Dichroic ratio measurements can be performed with dispersive IR spectrophotometers or with Fourier Transform Infrared Spectroscopy (FTIR) spectrometers. FTIR spectrometers show the multiplex advantage, where the signal-to-noise ratio of the spectra taken with the same resolution and the same measurement time is greater than that obtained on a grating instrument (27). Another advantage is the throughput (Jaquinot's advantage) that is greater for Michelson interferometers. However, in all IR measurements, in order to avoid deviations from Beer's law, it is required that the absorbance of the band to be smaller than 0.7 absorbance units, which is obtained by adjusting the thickness of the sample. Generally, it is possible to work with polymer samples with thicknesses between 1 and 200 μm. The choice of the absorption band is also a difficult task. The band should be well defined with no overlap with other absorption bands, it should belong to a functional group that conveniently describes the chain orientation, and it must be conformationally insensitive.

In recent years, the measurement of molecular orientation using infrared linear dichroism has been improved by the introduction of polarization modulation of the incident electromagnetic field (28). With this technique, it is possible to measure small dichroic effects with high sensitivity, even for very small draw ratios.

1.2.3. Birefringence

The birefringence Δ is defined as the difference in refractive index along two perpendicular axes. From this definition, it can be observed that three values of birefringence exist. In the case of uniaxial symmetry, only one value of birefringence has to be specified since the two values of refractive index orthogonal to the draw direction are equal. This technique gives an overall orientation, and using a combination of birefringence with other techniques of measurement of orientation, it is possible to obtain the chain orientation of individual components in a multicomponent system.

In the case of an oriented amorphous polymer, the relation between birefringence and the second moment of the orientation distribution function is given by:

$$\Delta = \Delta^\circ \langle P_2(\cos\theta) \rangle \qquad (11)$$

where Δ^0 is the intrinsic birefringence, and represents the birefringence for a perfectly oriented component. The refractive indices are correlated directly to the bond polarizabilities (29), which are related to the electron mobility in the three principal directions. For a multicomponent system,

$$\Delta = \sum_i f_i \, \Delta_i^0 \langle P_2(\cos\theta)_i \rangle + \Delta_F \qquad (12)$$

where Δ_F, is the form birefringence, a parameter related to the difference between the refractive index of the different phases, and f_i being the volume fraction of component or phase i.

The measurement of birefringence is simple but some conditions must be respected; the most important is the ability of the sample to transmit visible

radiation. In order to obtain birefringence as a function of draw ratio, the sample thickness must be known when the measurement is taken. If the measurement of thickness is not performed with enough accuracy, it is possible to use the approximation for uniaxial deformed rubbery systems:

$$d = d_o / \lambda^{1/2}$$
(13)

where d_o is the initial thickness of the sample, and λ is the draw ratio.

1.2.4. Doi-Edwards model

The Doi-Edwards (DE) theory (16 - 18) proved to be a successful theory for describing the polymer dynamics. A comprehensive review of this theory is given by Doi in Ref. 19. In a concentrated polymer solution, in which the chains are densely entangled, the mobilities of the chains are highly anisotropic. Each chain can move easily along its contour but the perpendicular motion to the chain contour is difficult. To express this situation, a hypothetical tube is introduced around each chain and represents the collective effects of the surrounding chains. It is considered that the motion of the tube is slower than the motion of the individual chain. The central line of the tube is called the primitive path or primitive chain (19). If L is the contour of the primitive chain with a step a (mean length between entanglements), and b is the bond length of the real chain, then the number of repeat units between entanglements N_e, can be calculated as:

$$N_e = \frac{a^2}{b^2}$$
(14)

and:

$$N = \frac{N_0}{N_e} \qquad (15)$$

where N is the number of entanglements per polymer chain and N_0 is the degree of polymerization of the polymer chain. The contour length of the polymer chain is given as:

$$L = aN = \frac{N_0 b^2}{a^2} \qquad (16)$$

If a step strain is applied, there is an increase in the contour length L and also a modification of the mean length between entanglements. At the macroscopic level, this produces a stress resisting the deformation or a modification in the second moment of the orientation distribution function. The Doi-Edwards model postulates the existence of three different relaxation processes:

1. The first is the Rouse-like relaxation of the segments between fixed entanglements, which does not change the value of L and a. The relaxation time is independent of the polymer molecular weight and is given as:

$$\tau_A = \xi b^2 N_e^2 / 6 \, \pi^2 k_B T \qquad (17)$$

where τ_A is the first relaxation time, k_B is the Boltzmann constant, T is the absolute temperature and ξ is the friction constant.

2. The second relaxation process occurs through the recoil of the chain ends into the deformed tube, modifying the contour length of the primitive chain L(t) to the equilibrium value L. From Eq. 15, it can be observed that a is also reduced. The

second relaxation process represents the relaxation of entanglement points, for which the corresponding relaxation time is:

$$\tau_B = \xi b^2 N_0^2 / 3\pi^2 k_B T \qquad (18)$$

3. The terminal relaxation process occurs through the reptation motions, removing the remaining orientation. This residual orientation resides in the persistent middle section of the initial deformed tube. The new sections of the primitive chain created by the reptating chains are isotropic in their spatial distribution. The relaxation time of the disengagement motions is given by:

$$\tau_C = \xi b^2 N_0^3 / \pi^2 k_B T \qquad (16)$$

In Fig. 2, an idealized sketch of the evolution of $\langle P_2(\cos\theta)\rangle$ in time is presented. As it can be observed for the case of an unentangled polymer, the relaxation behaviour is described by a single relaxation process only. For an entangled polymer, two other relaxation processes appear. As shown by Eqs. 15, 18 and 19, the second and the third relaxation times depend on the number of entanglements.
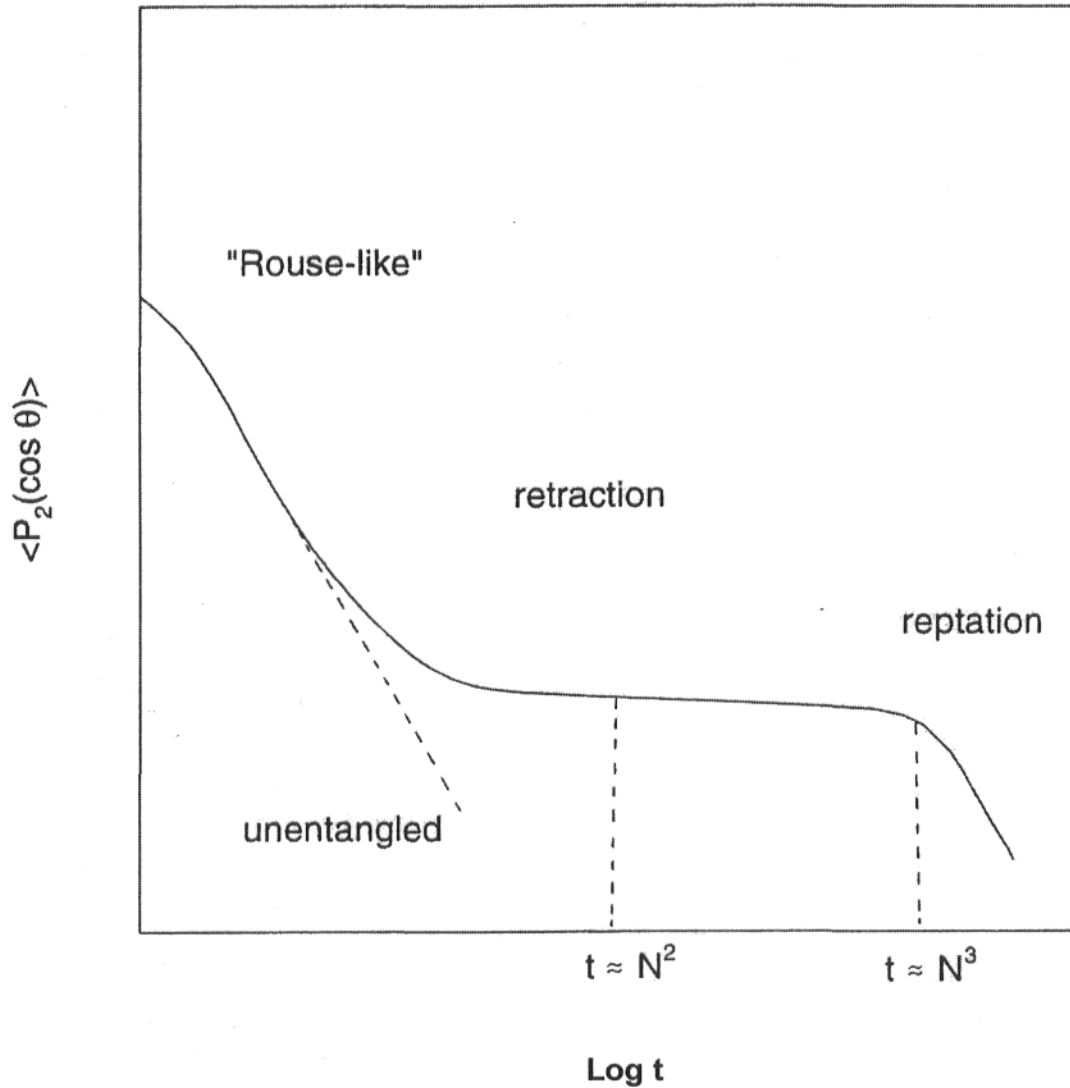
Figure 2:

Sketch of the relaxation of orientation for an entangled polymer. The "Rouse-like" motion is independent of molecular weight. The retraction process has a characteristic time scaling with N^2, whereas the reptation has a characteristic time scaling with N^3.

1.3 Objectives

The general objective of this mémoire is to study the molecular orientation of some polystyrene-based systems stretched uniaxially above their glass transition temperatures: the polystyrene homopolymer, poly(styrene-co-styrene sulphonic acid) (PS-SSA) copolymer containing 4.7 mol % SSA units, and a blend of PS-SSA (5.0% SSA) with poly(styrene-co-4-vinyl-pyridine) (PS-VP) (4.5% VP). The PS-SSA copolymer is characterized by strong H-bonding interactions among the SSA groups, and the blend by ion pair interactions created by proton transfer from SSA to VP.

The orientation behavior of these systems will be studied at different temperatures and different strain rates. For the case of polystyrene, an orientation-relaxation master curve will be drawn for exponential velocities of stretching.

The last part will be a confrontation between theory and experiment. Using the Doi-Edwards model, theoretical orientation curves will be drawn and compared with the experimental results. The relaxation times involved in the drawing of these curves will also be used for the simulation of relaxation curves after the deformation, and compared with experimental results.

The work presented in this mémoire was completed in 1995, and written as a Report. The above literature review covers the period up to this year. The last chapter of this mémoire, besides summarizing the main conclusions of the work accomplished, reviews the relevant literature subsequent to 1995. It also suggests directions that the present work could take in the light of the more recent literature, in particular using new methods for studying orientation and orientation relaxation that were developed after 1995.

2. Orientation Study of a Polystyrene Homopolymer, Copolymer and Blend

2.1. Sample Preparation

A polydisperse sample of PS, provided by Aldrich, with a weight-average molecular weight of 278,000 and number-average molecular weight of 119,000, determined with by Size Exclusion Chromatography with a Waters 590 Chromatograph using PS standards in THF, was purified by precipitation, adding dropwise a concentrated THF solution of PS into a large volume of stirred methanol, then soaked for one day. After a second washing with methanol, the wet PS was dried in an oven for ten days at 80°C.

The poly(styrene-co-styrene sulphonic acid) (PS-SSA) 4.7% was prepared by a standard method (30). Purified PS was dissolved in 1,2-dichloroethane. The sulphonation reagent was prepared adding 7.6 ml of acetic anhydride to 39.5 ml of 1,2-dichloroethane. The solution was cooled below 10°C, and 2.8 ml of 95% sulphuric acid was added, dropwise. Considering a conversion of 85%, 17 ml of sulphonation reagent was mixed with the PS solution, and maintained at 50°C for one hour with continuous stirring. The reaction was terminated with 7.2 ml of methanol. The resulting brown solution was added very slowly to boiling water under continuous stirring. The precipitated polymer was pulverized in a Waring blender and washed a few times with methanol, and finally filtered. The polymer was dried for one day at room temperature and, for at least eight days, at 60°C in a vacuum oven, until the values for the concentration of sulphonated PS, obtained by titration with sodium hydroxide, were constant. The conversion of sulphuric

acid to sulphonic acid was 80%. If the PS was not well dried and the used reagents were not fresh, the conversion could be much lower.

The blend of PS-SSA 5.0% with poly(styrene-co-4-vinyl-pyridine) (PS-VP 4.5%) was previously prepared in connection with an earlier project (12) by dissolving the copolymers separately in THF/methanol (90/10) solutions, following which the PS-VP solution was added dropwise to the vigorously stirred PS-SSA solution. The gel-like compound was precipitated in methanol and further dried in a vacuum oven at room temperature for one day and at 120° C for three days.

Thin films of uniform thickness ($\pm$ 2 μm), with thicknesses between 40 and 70 μm, were prepared at about Tg+50°C, using a SPECAC-IR film-making mold, under a pressure of 5000 psi for 3 min. The films were cut into strips of 5 mm width and 200 mm length. At each end, pyro-tape (1/2", #546, Aremco Products Inc.) was fixed in order to prevent slippage during the stretching. Thin ink lines were drawn at every 5 mm in order to check if the drawing was constant throughout the film. The film samples were dried for 24 h at 60°C in a vacuum oven before measurement.

2.2. DSC Measurements

The glass transition temperature (Tg) was measured with a Perkin Elmer differential scanning calorimeter, DSC-4, calibrated with indium, at a heating rate of 20°C/min, with a sample weight of about 15 mg. The Tg values, taken as the midpoint of the heat capacity jump, are presented in Table 1.

Table 1: Glass transition temperatures for the investigated polymers

Polymer	Source	Tg(°C)
PS	Aldrich	104
PS-SA (4.7 %)	Sulphonation of Aldrich PS	112
PSSA (5.0 %)/ PS-VP (4.5 %)	See text	115

2.3. Stretching Conditions

The stretching was performed with a home-made stretching device that has a fixed lower clamp. During the stretching, the upper clamp was raised at different exponential velocities, giving a constant strain rate. Various draw ratios were chosen and, before stretching, the samples were allowed to stay at the stretching temperature for 10 min. After stretching, for orientation measurements, the sample was quickly quenched to room temperature by opening the front door of the stretching device and, using a fan, effectively freezing the orientation of the polymer. For the relaxation measurements, after the stretching, the samples were held in the stretching apparatus at a fixed strain, at the stretching temperature, for different periods of time. The draw ratio was limited to four in order to prevent the breaking of the samples. The samples were carefully selected as a function of their thickness, so that, after the stretching at different draw ratios, all samples had approximately the same thicknesses.

2.4. Orientation Measurements

FTIR orientation measurements were performed at room temperature by recording pairs of polarized spectra with a Mattson FTIR Spectrometer (SIRIUS 100) equipped with a MCT detector. The resolution was 4 cm^{-1} and 100 interferograms were accumulated. To obtain parallel and perpendicular spectra to the direction of stretching, a wire grid polarizer was used and the samples were rotated 90°C with a home-made motorized device. Three or more sets of data were obtained in the middle of the areas where the draw ratio was strictly respected. The analyzed bands were always kept in the linear region of absorbance. The two PS bands most frequently used for orientation measurements are at 906 and 1028 cm^{-1}. The band at 1028 cm^{-1} is attributed to the ν_{18a} in-plane CH bending mode of the benzene ring, with an angle a of 90° (31). For this band, Eq. 10 becomes:

$$\langle P_2(\cos\theta)\rangle = 1/2\left(3\cos^2\theta - 1\right) = 2\times\left[(R-1)/(R+2)\right] \tag{20}$$

The band at 906 cm^{-1} corresponds to the out-of-plane ν_{17b} mode of the benzene ring. With the angle a determined to be 35° (31), Eq. 10 becomes:

$$\langle P_2(\cos\theta)\rangle = 1/2\left(3\cos^2\theta - 1\right) = 1.97\times\left[(R-1)/(R+2)\right] \tag{21}$$

Birefringence measurements were performed with a Carl Zeiss polarizing microscope, using an Ehringhaus rotary compensator with quartz combination plates. The measuring range of the compensator extends either side of the zero position. For exact measurements, the setting was made toward both sides, and

18

the arithmetic mean of the readings was calculated. For measurements, a filter with maximum transmissivity band between 530 and 560 nm was used. The calculation of the phase difference was carried out using the 546.1 nm spectral line with the formula:

$$\Gamma_\lambda = \left(\varepsilon^2 - \sin^2 i\right)^{1/2} - \varepsilon/\omega\left(\omega^2 - \sin^2 i\right)^{1/2} \qquad (22)$$

where Γ_λ is the phase difference at the wavelength λ, $\omega = 1.546168$ and $\varepsilon = 1.555339$ are the refractive indices of the ordinary and extraordinary wave in the quartz for the wavelength λ, and i is the angle of inclination of the plane of the quartz plate relative to its 0 position. The birefringence was obtained using the relation:

$$\Delta = \Gamma_\lambda/d \qquad (23)$$

where d is the sample thickness. Each birefringence value determined is an average of the measurements taken from three or more samples stretched at the same draw ratio.

2.5. Results and Discussion

2.5.1. Pure Polystyrene

The orientation behaviour of PS was studied at five different temperatures, Tg+10°C, Tg+15°C, Tg+20°C, Tg+25°C, and Tg+30°C, and at four different strain rates, 0.026 s^{-1}, 0.052 s^{-1}, 0.10 s^{-1} and 0.30 s^{-1}. The 1028 cm^{-1} band was used to calculate the orientation. As shown in Figs. 3 to 7, the orientation function

increases linearly, as expected, with the draw ratio at all temperatures and strain rates. Increasing the temperature of stretching gives a decrease in the orientation when the comparison is done at the same strain rate. As seen from Eqs. 17, 18 and 19, the relaxation times have smaller values at higher temperatures. For a given temperature of stretching, it is observed that the orientation increases with the strain rate. This is an expected result since the relaxation times, τ_A, τ_B, and τ_C, do not depend on the strain rate, and the stretching is performed in a shorter period of time at higher strain rates. It can also be observed that an increase in strain rate has the same effect as a decrease in the temperature.

As mentioned in Refs. 32 and 33, the influence of temperature and strain rate obeys the time-temperature superposition principle. That means that the orientation measured at a certain draw ratio for a strain rate ε_1 and a temperature T_1, is identical to that obtained at strain rate ε_2 and temperature T_2. In these conditions, it is possible to build a master curve of orientation for a given draw ratio. In Ref. 34 the master curve was constructed considering that:

$$\varepsilon_2 = \varepsilon_1 / a(T_2/T_1) \tag{24}$$

where the shift factor $a(T_2/T_1)$ is given by the WLF equation:

$$\log a(T_2/T_1) = A(T_2 - T_1)/(B + (T_2 - T_1)) \tag{25}$$

In Ref. 34, it was possible to use directly Eq. 24, since the strain rate, for a constant velocity of stretching, is the reverse of stretching time. For the case of an exponential velocity of stretching, the stretching time is defined as:

$$t = 1/\varepsilon \times \ln \lambda \tag{26}$$

Figure 3:

Molecular orientation of PS for different strain rates at 114°C

T = Tg + 10°C
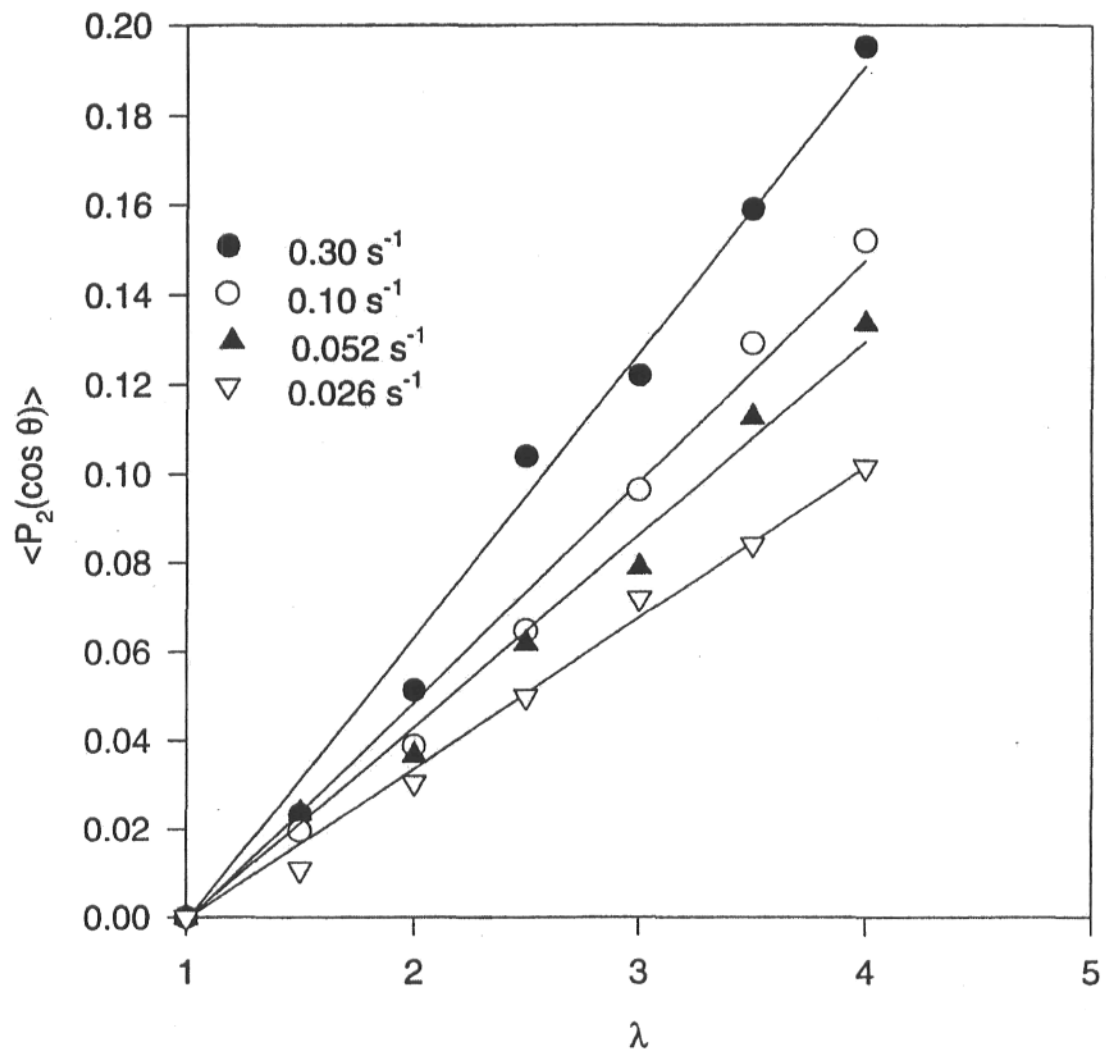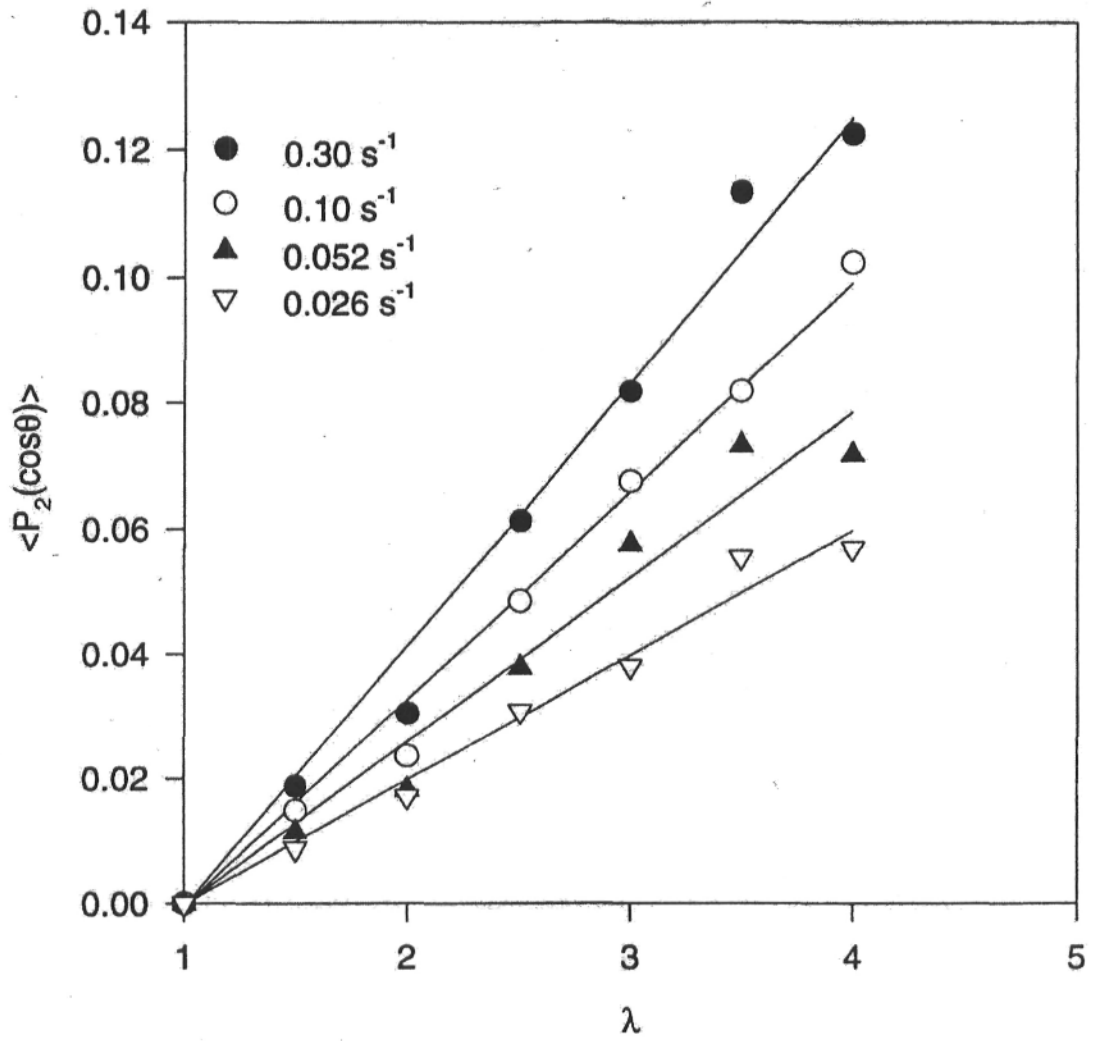
Figure 4:

Molecular orientation of PS for different strain rates at 119°C

T = Tg + 15°C
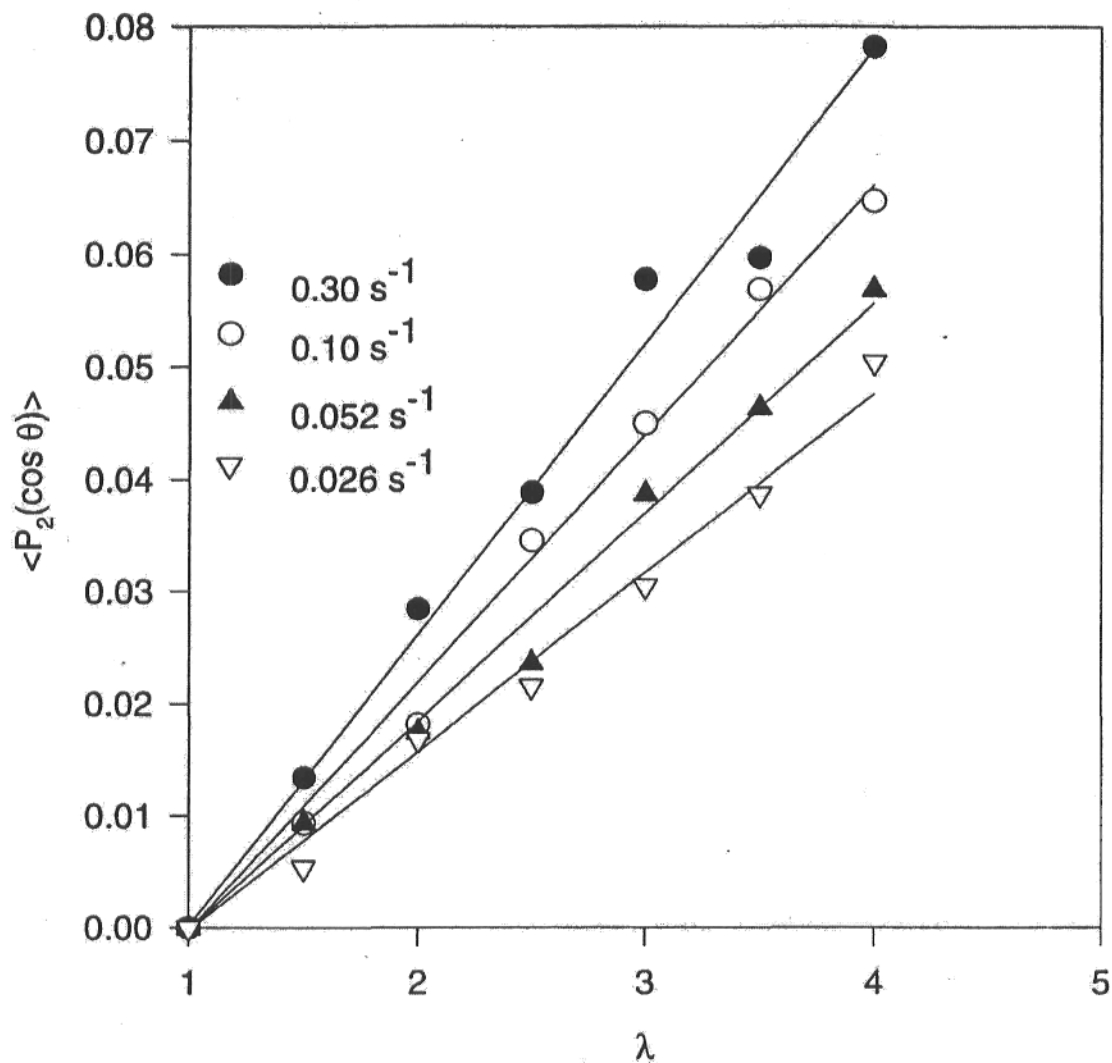
Figure 5:

Molecular orientation of PS for different strain rates at 124°C

T = Tg + 20°C
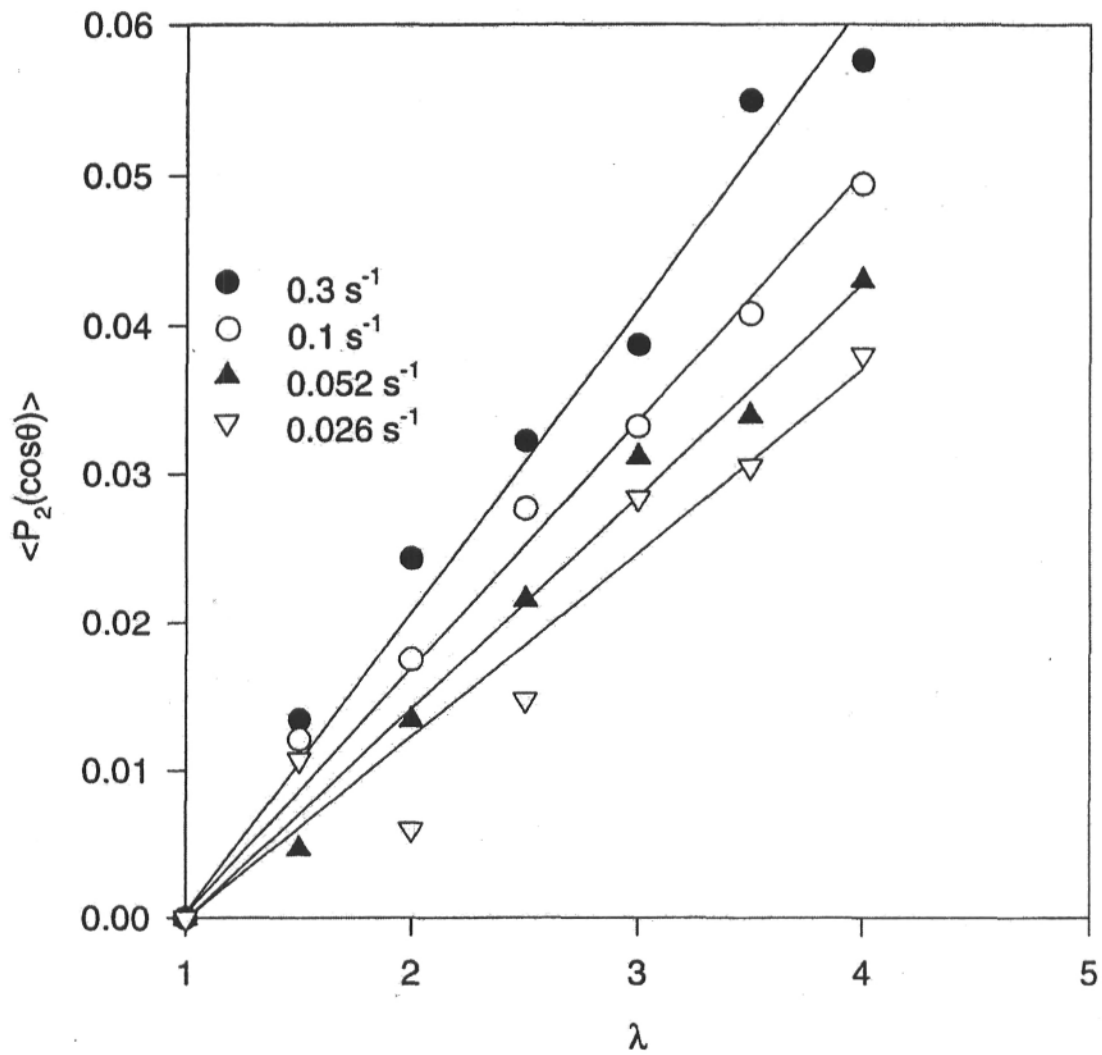
Figure 6:

Molecular orientation of PS for different strain rates at 129°C

T = Tg + 25°C
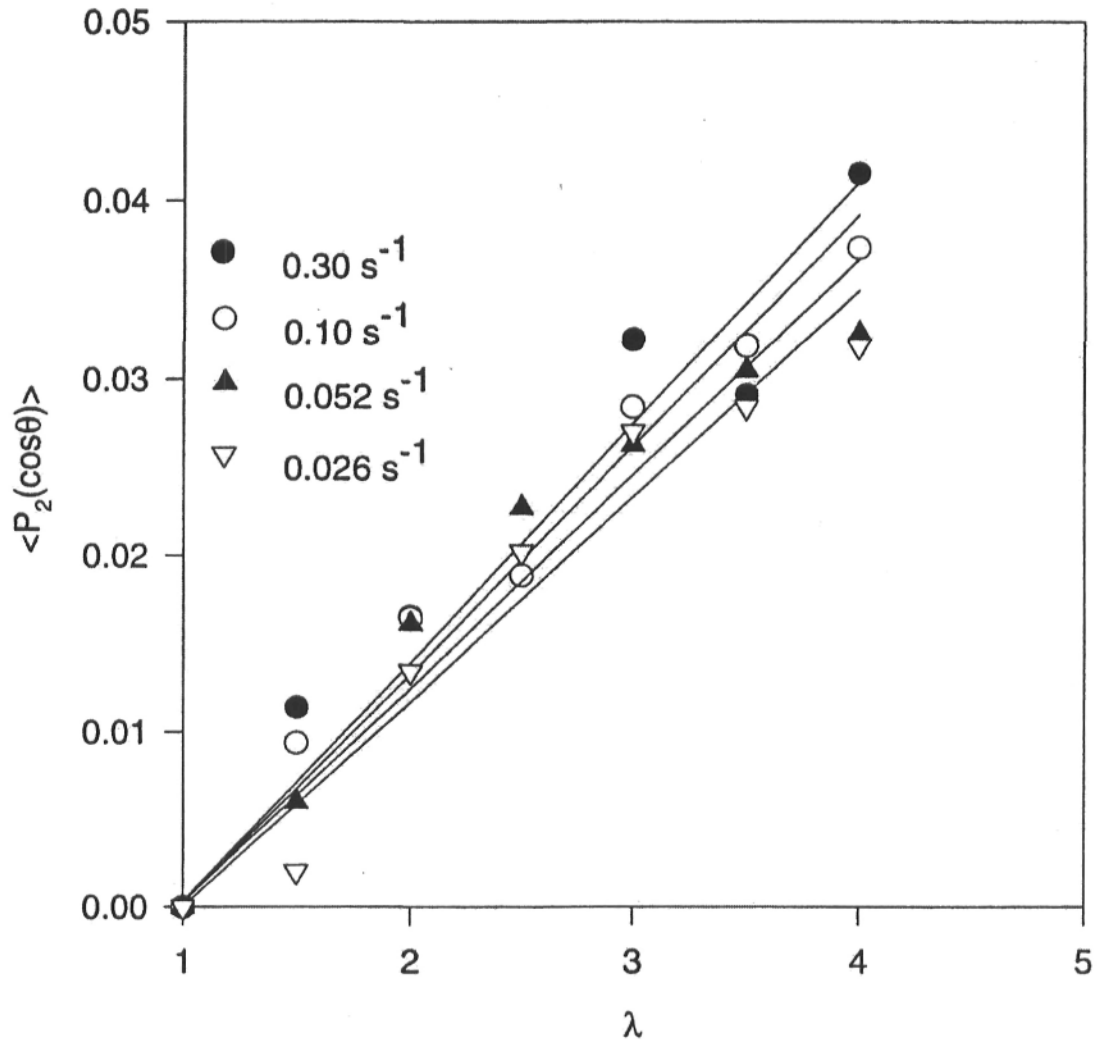
Figure 7:

Molecular orientation of PS for different strain rates at 134°C

T = Tg + 30°C

where λ is the draw ratio. In Fig. 8, the values of orientation, for a draw ratio $\lambda=4$, taken from Figs. 1 to 5, are plotted versus stretching time. For a reference temperature of 120°C, and the values for the two coefficients A = - 9.06, B = 68.3°C (32) and, using the relation:

$$t(T_1) = t(T_2)/a(T_2/T_1) \tag{27}$$

it is then possible to obtain, from Fig. 8, an orientation relaxation master curve. As shown in Fig. 9, it can be observed that the data obtained under different conditions of temperature and at different stretching times superpose rather well. The results in Fig. 9 show that the principle of time-temperature superposition applies for orientation measurements at exponential velocities of stretching. This kind of representation for orientation measurements becomes more meaningful when secondary axes are drawn for a given reference strain rate, showing what the orientation is if the temperature changes or, for a given reference temperature, showing what the orientation is if the stretching rate is modified. This curve suggests also that the relaxation times for different temperatures are correlated with one another by WLF coefficients. The orientation-relaxation master curve obtained for exponential velocities of stretching has a similar shape with the master curve from Ref. 34 that was obtained for constant velocities of stretching. This fact suggests that the orientation values, obtained after a deformation step, depend on the stretching time rather on the type of the velocity used for stretching.
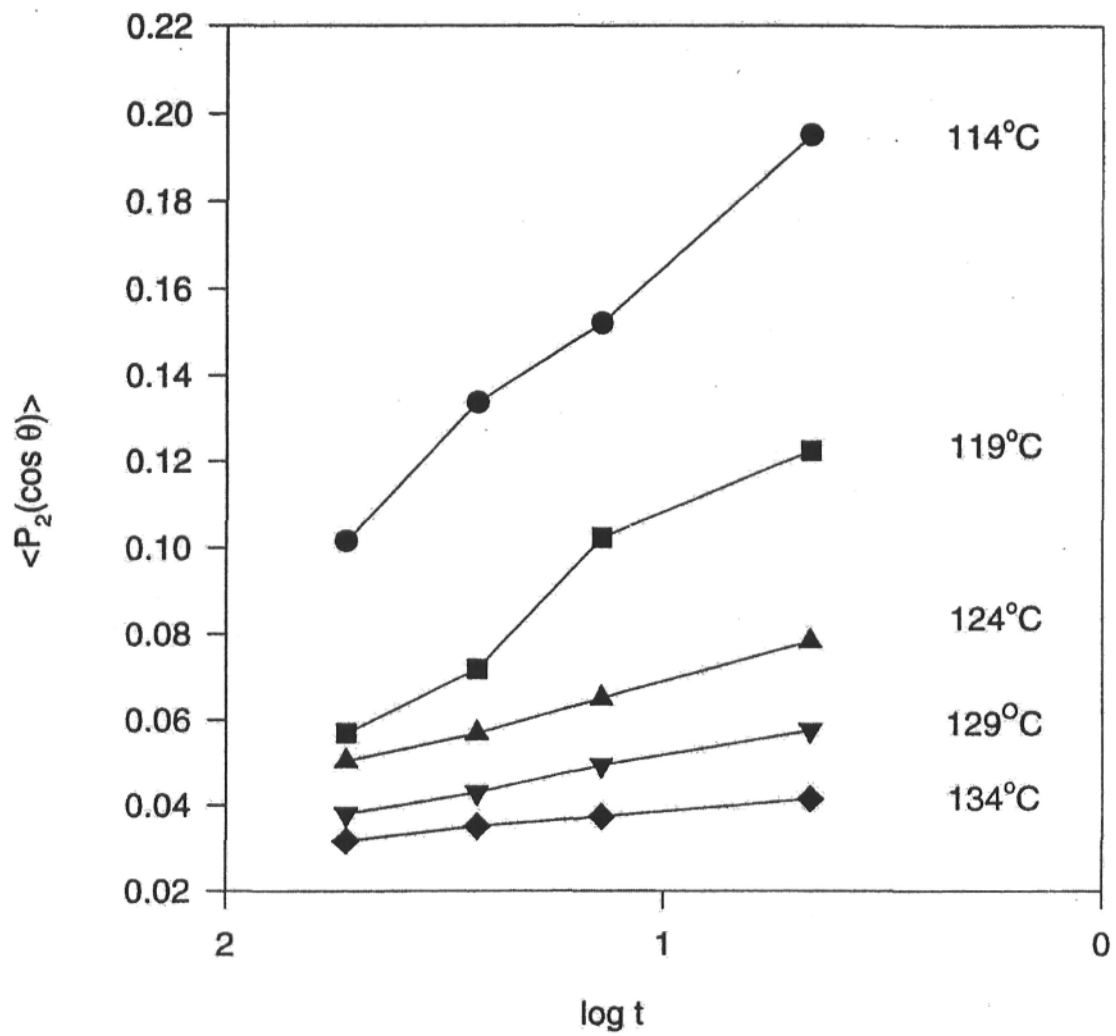
Figure 8:

Orientation behaviour of PS as a function of the stretching time
at five different temperatures
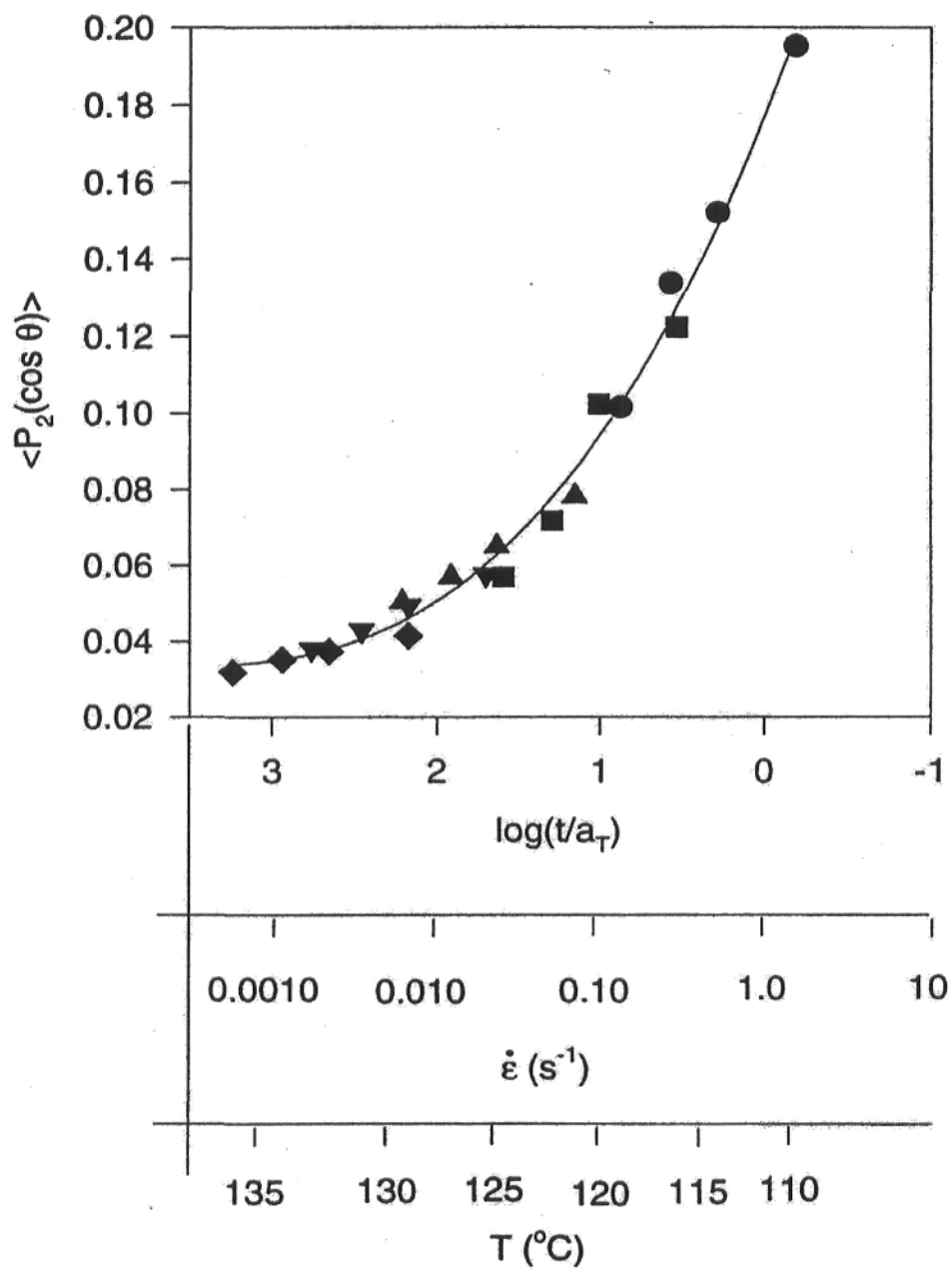
Figure 9:

Orientation - relaxation master curve for a PS sample

2.5.2. Poly (styrene co-styrene sulphonic acid) copolymers

The molecular orientation behaviour of PS-SSA copolymers, as well as the orientation of neutralised PS-SSA copolymers, were previously studied in our group (10, 11). It was observed that the orientation increases significantly with SSA content (10), and, as seen in Fig. 10 for the 1028 cm^{-1} band, the increase in orientation with draw ratio is not linear for acid contents of 7% or higher. The presence of sulphonic acid groups enhances the orientation, which behaviour can be explained taking into consideration the hydrogen bonding interactions between them (9). These interactions can act as effective crosslinks or can slow down the chain relaxation during the deformation process.

Based on dynamic mechanical and small angle X-ray scattering data, there are different opinions (35, 36) as to whether sulphonic acid groups in PS-SSA aggregate to form multiplets or even clusters. For accurate determinations of P_2 values, some complications with PS-SSA were encountered. The PS-SSA copolymers are easily hydrated, as can be detected from infrared spectra by the presence of bands at 1004 and 1128 cm^{-1}. The presence of water molecules that intervene in the acid associations may affect the orientation. For the highest acid contents, it is difficult to verify if there are traces of water, since the samples are subject to degradation during prolonged drying.

A second problem is the band used for P_2 determinations. The 1028 cm^{-1} band is preferred to the 906 cm^{-1} band since, in the lower wavenumber side of the 906 cm^{-1} band there is a shoulder attributed to the single bond S-O stretch of the acid group (10). It was noted (10) that the 1028 cm^{-1} band could be affected by the SSA content since the hydrated SSA groups, in completely sulphonated PS, should give rise to a symmetric stretching vibration of the SO_3^- ion produced at

1034 cm^{-1}. Also, the 2850 cm^{-1} band could be influenced by the SSA content (11) because of stretching vibrations arising from SO_3H and/or H_2O.

In order to verify if the previous orientation measurements for PS-SSA copolymers (up to 5 mol %) are correct, their orientation behaviour was studied using birefringence. The evolution of the orientation of the PS-SSA 4.7% as a function of draw ratio for samples stretched at 127°C (Tg+15°C), for the 1028 cm^{-1} band, is given in Figure 11. It can be observed that the orientation function increases linearly with the draw ratio. The birefringence behaviour versus draw ratio for the same set of samples is drawn in Fig. 12. Birefringence linearly increases with the draw ratio. Fig. 13 gives a plot of the birefringence values from Fig. 12 versus orientation values from Fig.11 at the same draw ratios. From the slope, it is possible to calculate the intrinsic birefringence, as given by Eq. 10. The value of -0.110 ± 0.005 obtained from the slope is slightly higher than that reported for PS (9), which is -0.100 ± 0.005. The fact that the slopes for PS and for PS-SSA are almost identical indicates that the measurements for the latter are not influenced within the experimental error of the orientation measurements by the possible complications of H_2O on the 1028 cm^{-1} band up to 4.7 mol %. Thus the previous results using infrared dichroism are validated.

In this comparison, the experimental error has to be taken into account, as well as the fact that the intrinsic birefringence of PS exhibits a large variation since it depends on the average angle <α> between the normal to the benzene ring and the principal axis of the chain, as it is given by the theoretical relation developed by Stein (29):

$$\Delta_{PS}^0 = 0.194 - 0.51\langle\cos^2 \alpha\rangle \tag{28}$$

For the angle $<\alpha>$, the values found in the literature range between 34 and 38° (31), and can be as high as 47° (37). From these considerations, it would be interesting to compare the orientation results from infrared measurements with the birefringence values for different SSA contents. A plot of intrinsic birefringence versus SSA content could set the concentration limits for which the 1028 cm^{-1} band can be used.

As in the case of PS, the behaviour of the orientation function of PS-SSA 4.7% was studied as a function of the temperature and strain rate. From Figure 14, it is observed that the orientation increases with higher strain rates. The explanation is the same as in the case of PS that, at higher strain rates, there is a smaller amount of time for the relaxation of orientation. The influence of temperature above Tg on orientation measurements is indicated in Fig. 15. From Figs. 14 and 15, one can see that an increase in strain rate has the same effect as a decrease of temperature. Because of insufficient data, it was not possible to determine the WLF coefficients and, to our knowledge, these coefficients are not available in the literature. For this reason, a master curve was not built for this blend.
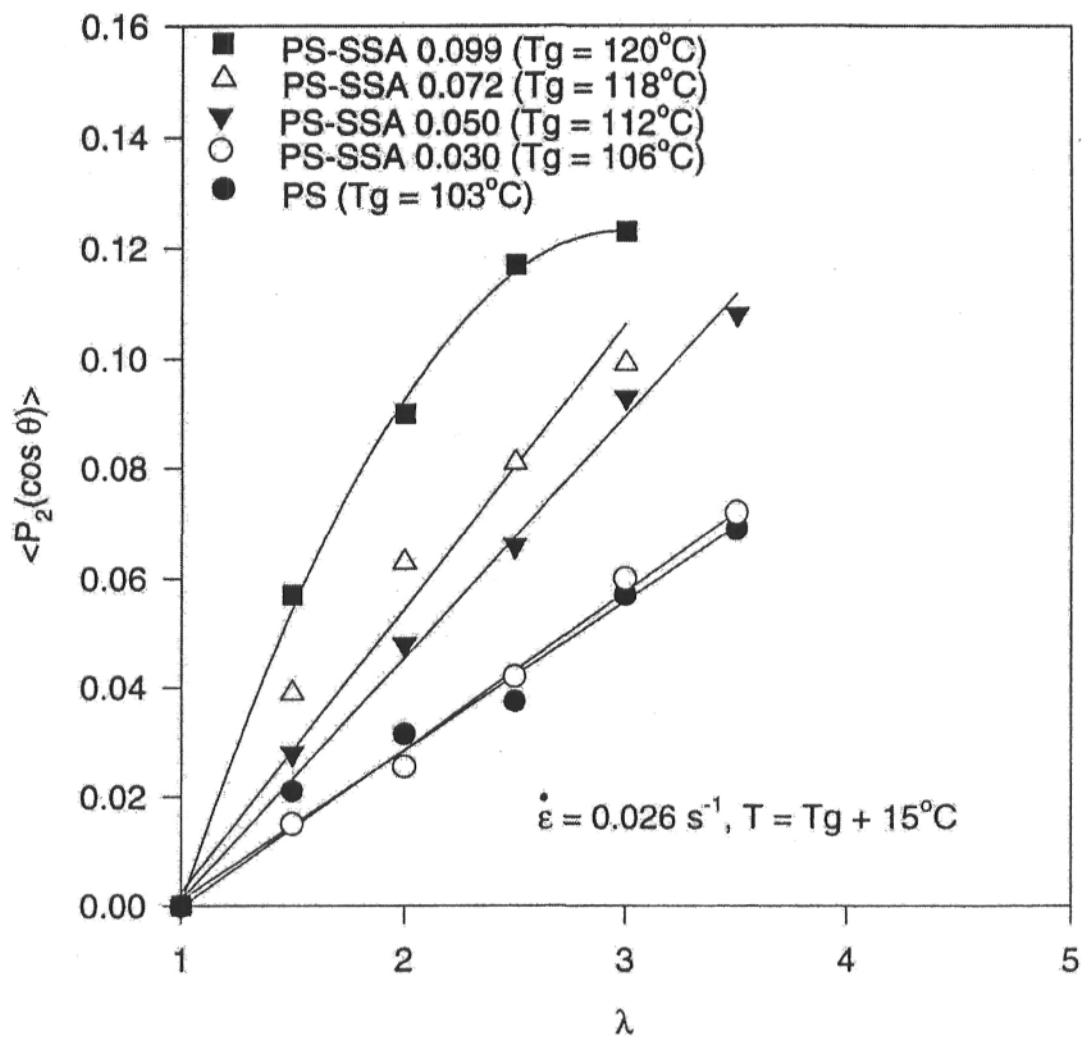
Figure 10:

Molecular orientation of PS and PS-SSA copolymers of
different SSA mole fractions
(with permission from Ref. 10)
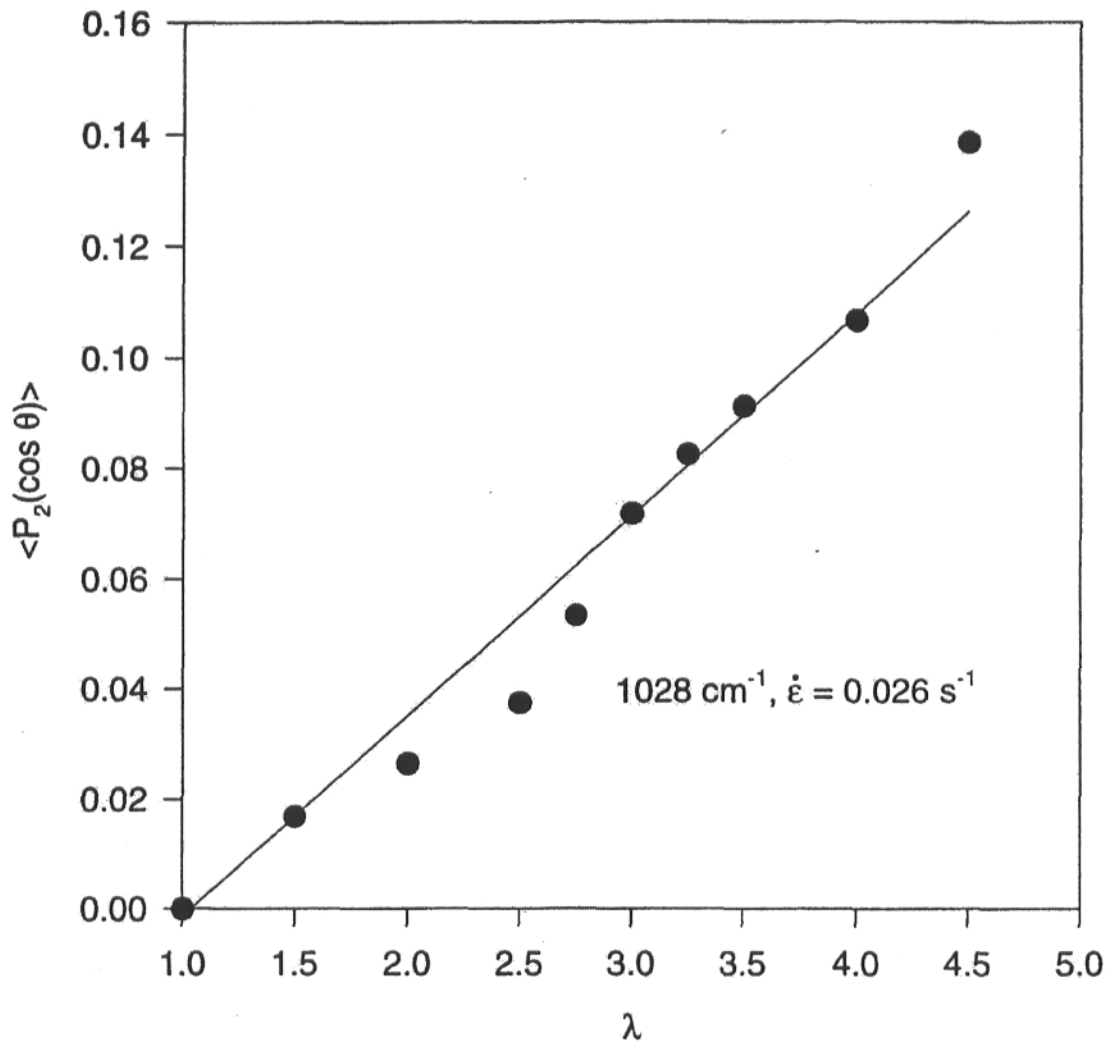
Figure 11:

Molecular orientation of PS-SSA 4.7% at 127°C (Tg + 15°C)
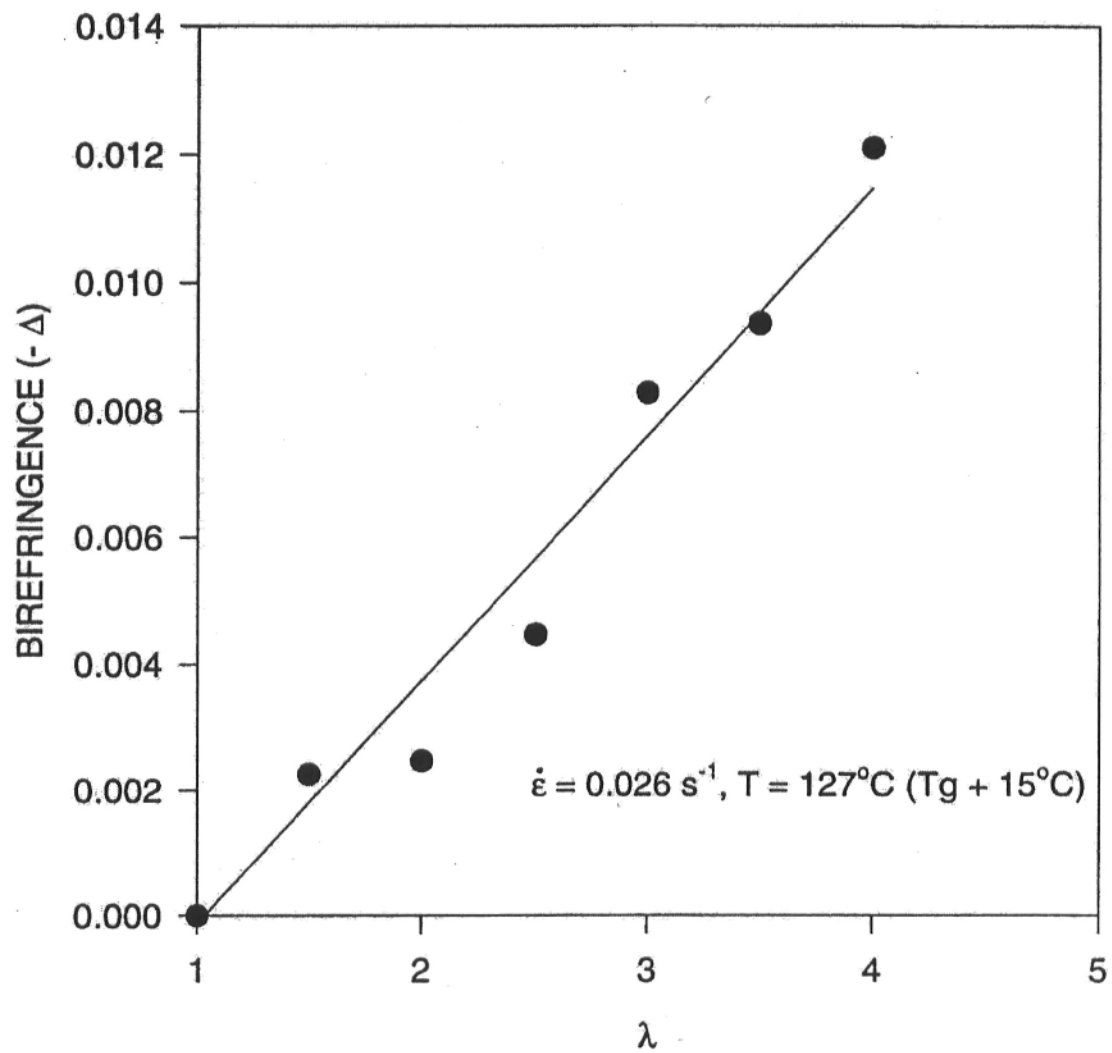
Figure 12:

Birefringence of PS-SSA (4.7%) as a function of the draw ratio
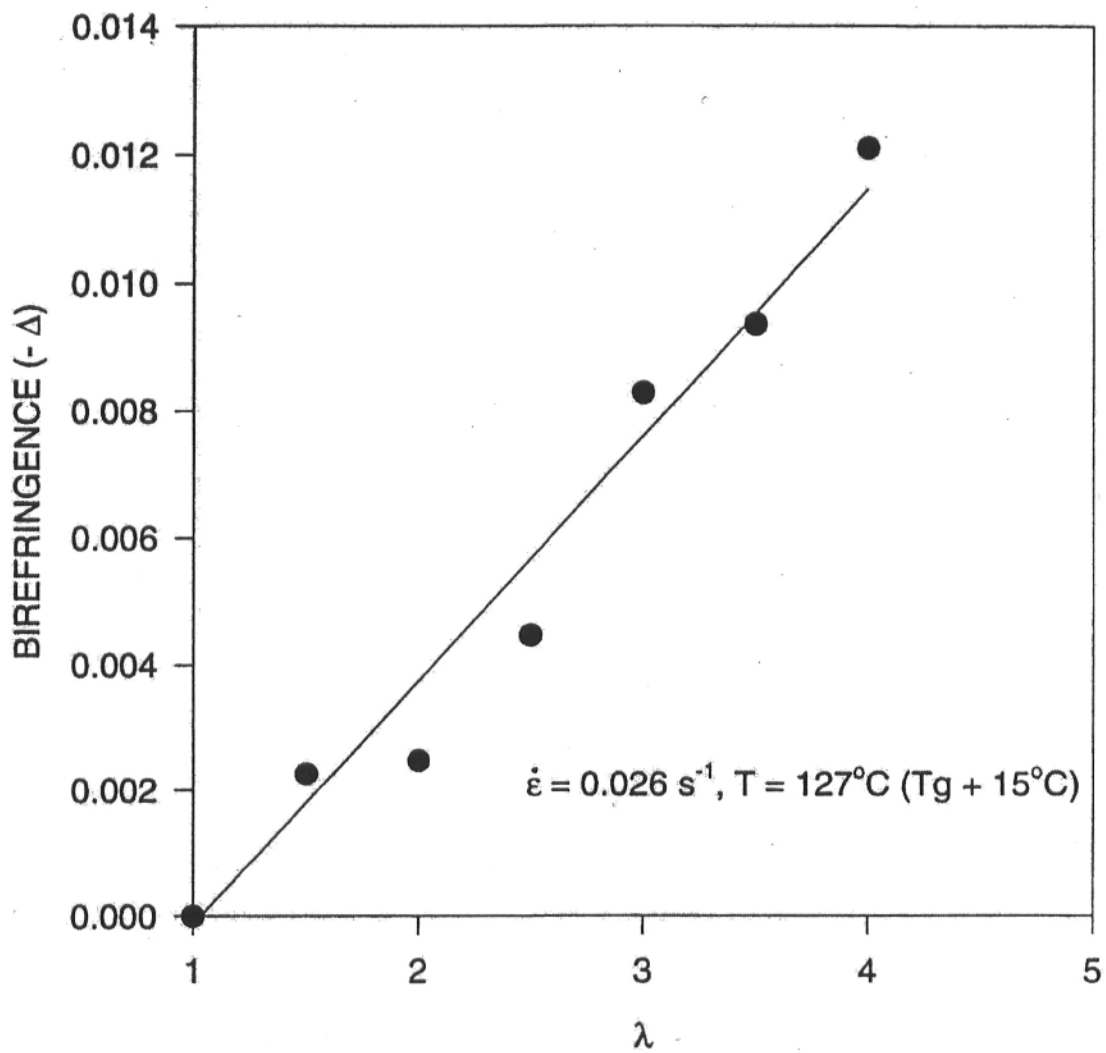
Figure 13:

Molecular orientation of PS-SSA 4.7% vs birefringence
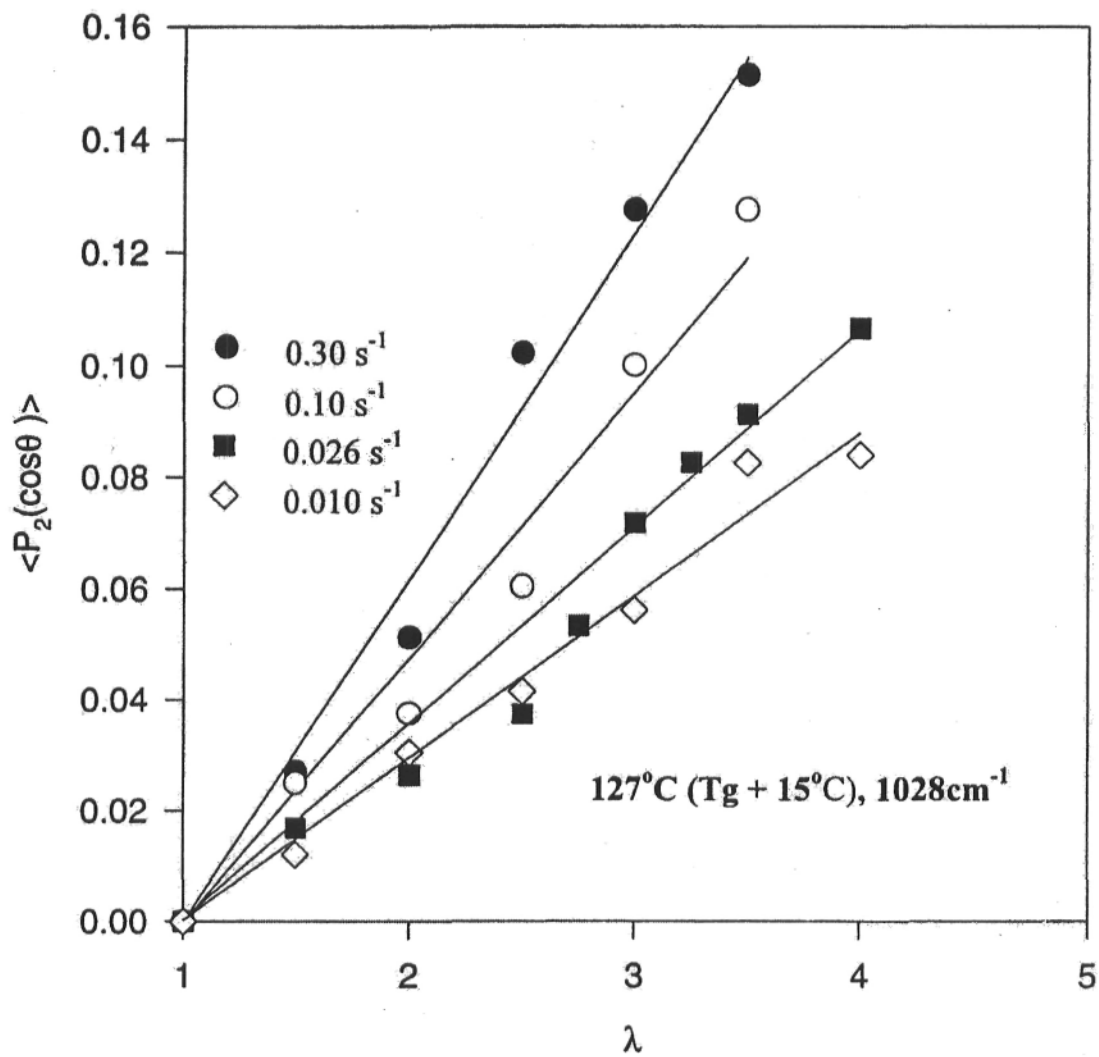
Figure 14:

Molecular orientation of PS-SSA 4.7 % at different strain rates
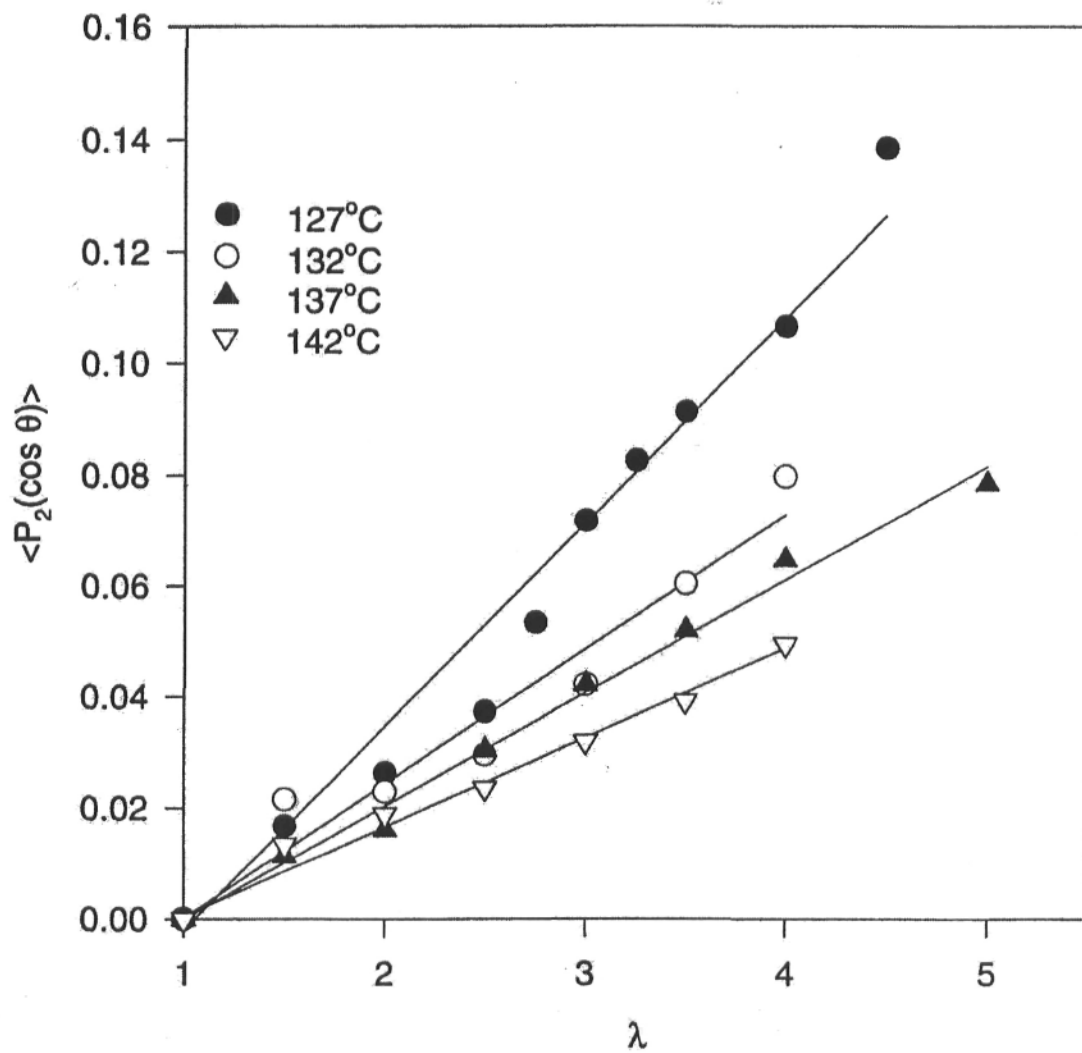
Figure 15:

Molecular orientation of PS-SSA 4.7 % at different temperatures

2.5.3. Blend of PS-SSA (5.0% SSA) with Poly(styrene-co-4-vinyl-pyridine) (PS-VP) (4.5% VP)

For the case of PS-SSA/PS-VP blends, the orientation measurements were taken using the 906 cm^{-1} band because the intensity ratio of the 1028/1945 cm^{-1} bands (1945 cm^{-1} serving as the internal standard) differs significantly from that of PS due to ionization of SSA, whereas the ratio of the 906/1945 cm^{-1} bands shows no difference in comparison with PS (10) since the acid group has been eliminated by the ionization. As in the cases of PS and PS-SSA 4.7%, the orientation behaviour was studied at different strain rates. From Fig. 16, it is observed that, for a shorter stretching time, the orientation increases. For temperatures of stretching above their glass transition, the measured orientation values are much higher for the blends than those of their acid precursors or parent homopolymers (8, 38). This is observed in Fig. 17, where at Tg + 20°C and at the same strain rate, the orientation of PS-SSA (5.0%)/PS-VP (4.5%) is shown to be higher than those of PS-SSA 4.7% and of PS. Also, it was observed that the orientation increases with the co-unit content (10) meaning that the proton transfer from the acid to the pyridine, leading to the ion-ion interactions (24), causes an enhancement of orientation.

This behaviour could be explained taking into account that the pyridinium-sulphonate interactions could act as crosslinks, or could slow down the chain relaxation by an increase in the friction coefficients. From Eqs. 17, 18 and 19, it is observed that an increase in the friction coefficients would proportionally increase all the relaxation times. In practice (10), it was observed that the relaxation behaviour is quite similar in the region of the first relaxation process for different compositions, even if the second and the third relaxation processes seem to be slower for higher ion content (10).
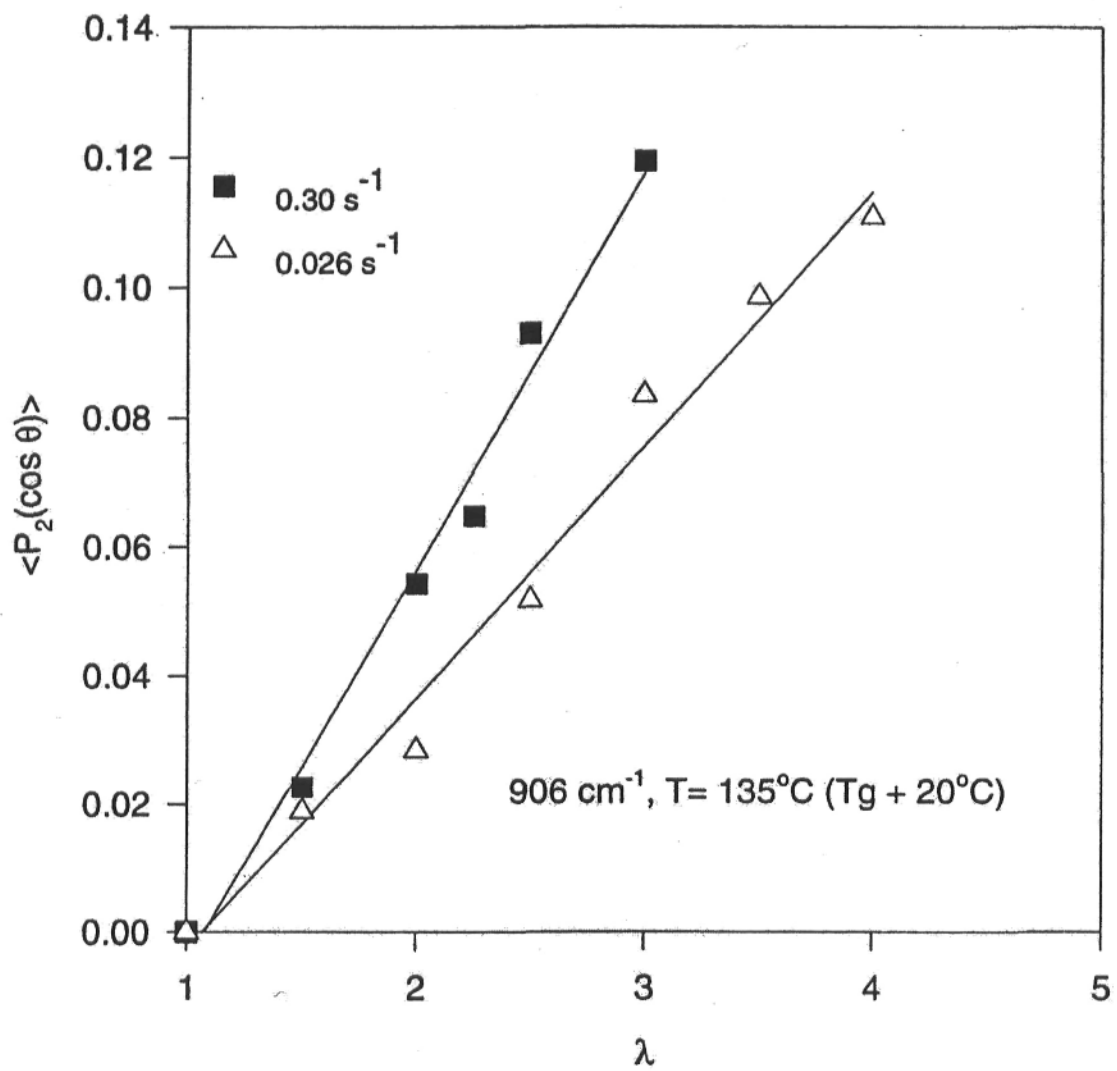
Figure 16:

Molecular orientation of PS-SSA 5.0%/PS-VP 4.5%

at different strain rates
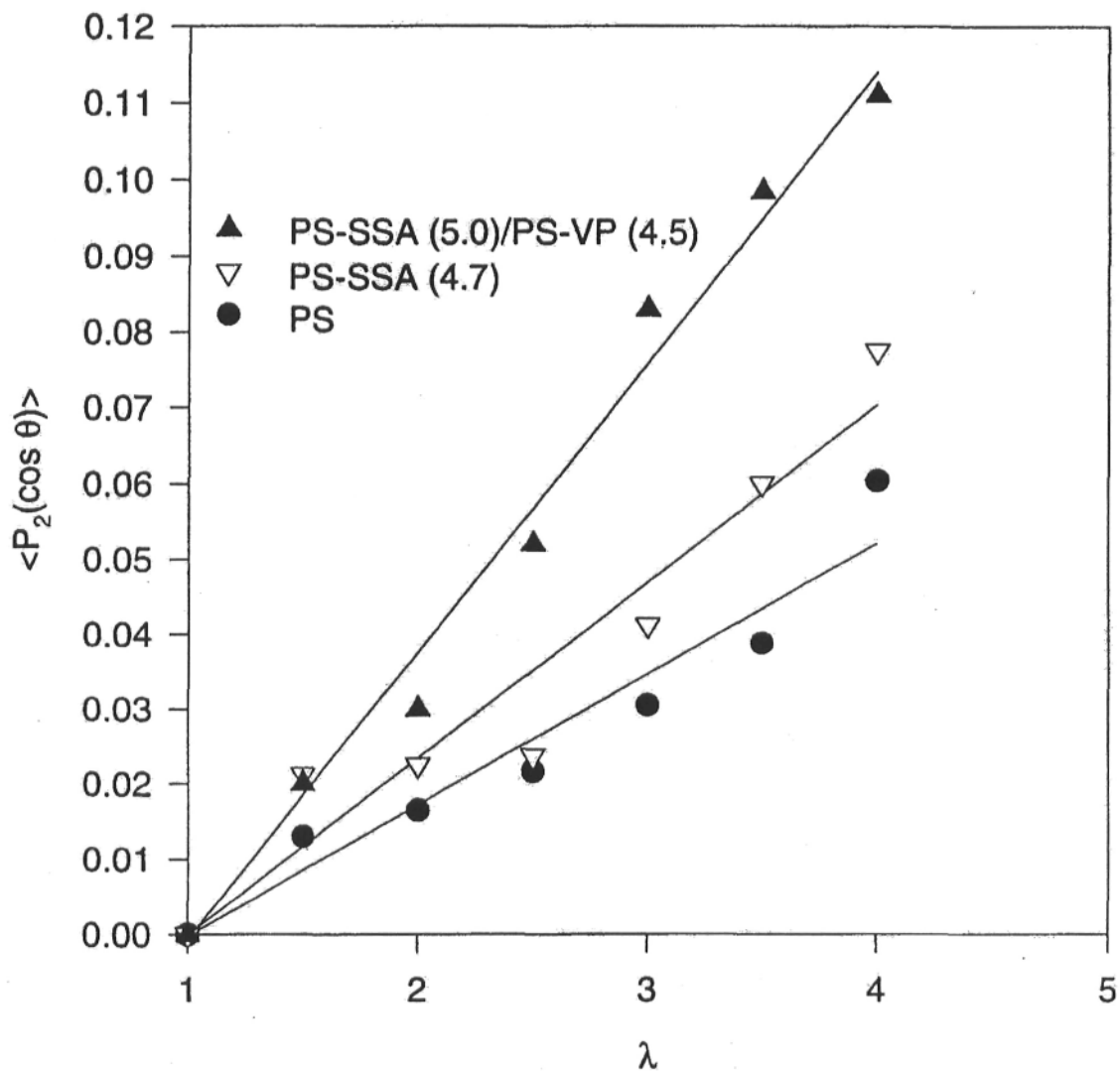
Figure 17:

Molecular orientation of PS, PS-SSA (4.7%), PS-SSA 5.0%/PS-VP 4.5%
at the indicated strain rates and 135°C (Tg +20°C)

Starting with this observation, it is considered that the orientation behaviour of PS-SSA/PS-VP blends is primarily due to crosslinking effects. Also, there are some data in the literature (9) leading to the conclusion that clusters exist in this kind of blends that could act as multifunctional crosslinks (8, 11).

In order to give a more exact response about the relation between the relaxation times of PS-SSA/PS-VP blends of different compositions, more detailed investigations on the relaxation of orientation for different domains of time are necessary.

3. Analysis of Orientation Using the Doi-Edwards Theory

As summarized in the introduction, the Doi-Edwards theory offers a simple description of the relaxation motions using a small number of parameters. Tassin (33) used this model to study the relaxation of orientation study after a step deformation. In our group, the Doi-Edwards topological model was extended for the study of molecular orientation in blends (37). According to Ref. 33, the relaxation of orientation following a step deformation of amplitude λ is given by:

$$P_2(t) = P_2^{network}/\alpha^2(\lambda)\mu_A(t)g^2(t/\tau_B)\mu_C(t) \tag{29}$$

where:

$$g(t/\tau_B) = 1 + (\alpha(\lambda) - 1)\mu_B(t) \tag{30} \qquad X = (\lambda^3 - 1)^{1/2} \tag{32}$$

$$\alpha(\lambda) = (\lambda + \sinh^{-1} X/(X\lambda^{1/2}))/2 \tag{31} \qquad P_2^{network} = 1/5n_K(\lambda^2 - 1/\lambda) \tag{33}$$

where $P_2^{network}$ represents the orientation at the end of the stage A ($\tau_A < t < \tau_B$), n_k is the average number of statistical Kuhn segments between slip-links, λ is the amplitude of the deformation and $\mu_A(t), \mu_B(t)$, and $\mu_C(t)$, are defined by:

$$\mu_A(t) = 1 + \sum_1^{Nr} \exp(-tk^2/\tau_A) \tag{34}$$

$$\mu_B(t) = \sum_{p\,odd}(8/p^2\pi^2)\exp(-tp^2/\tau_B) \tag{35}$$

$$\mu_C(t) = \sum_{p\,\text{odd}} \left(8/p^2\pi^2\right) \exp\left(-tp^2/\tau_C\right) \tag{36}$$

From Eqs. 17-19, it can be written that:

$$\tau_B = 2\tau_A \left(M_i/M_e\right)^2 = 2\tau_A \left(N_0/N_e\right)^2 \tag{37}$$

$$\tau_C = 6\tau_A \left(M_i/M_e\right)^3 = 6\tau_A \left(N_0/N_e\right)^3 \tag{38}$$

where M_i is the molecular weight, and M_e the molecular weight between entanglements. Following the approach adopted by Tassin in the calculation of the applied stress, Eq. 29 was rewritten (37) in the form:

$$P_2(\lambda, t) = c \sum_{i=1}^{3} F_i(\lambda)\mu_i(t) \tag{39}$$

where c is a constant related to the density between entanglements. It has the form given by (37):

$$c = 3/\left(5n_K\right) \tag{40}$$

$F_i(\lambda)$ and $\mu_i(t)$ are given by:

$$F_1(\lambda) = \left(1/3\alpha^2\right)\left(\lambda^2 - 1/\lambda\right) \tag{41}$$

$$\mu_1(t) = \mu_A(t)\mu_C(t) \tag{44}$$

$$F_2(\lambda) = \left(2/3\alpha^2\right)\left(\alpha - 1\right)\left(\lambda^2 - 1/\lambda\right) \tag{42}$$

$$\mu_2(t) = \mu_A(t)\mu_B(t)\mu_C(t) \tag{45}$$

$$F_3(\lambda) = 1/3(1 - 1/\alpha^2)(\lambda^2 - 1/\lambda) \quad \textbf{(43)} \qquad\qquad \mu_3(t) = \mu_A(t)\mu_B^2(t)\mu_C(t) \qquad \textbf{(46)}$$

where $\mu_A(t)$, $\mu_B(t)$, and $\mu_C(t)$ are given in Eqs. 34-36.

For an exponential strain rate, and assuming the validity of the Boltzmann superposition principle, the second moment of the orientation function can be written (33):

$$P_2(\lambda, t) = -\sum_{i=1}^{3} \int_{-\infty}^{t} \mu_i(t - t')\, d[F_i(\lambda, \lambda')]\, dt' \qquad \textbf{(47)}$$

where:

$$F_i(\lambda, \lambda') = F_i(\lambda(t)/\lambda'(t')) \qquad \textbf{(48)}$$

For the case of an exponential velocity of stretching, $\varepsilon = (\ln\lambda)/t$, the limiting conditions are:

$$t \leq 0,\ \lambda = 1 \qquad\qquad\qquad (\lambda, \lambda') = \lambda(t),\ \text{if } t' \leq 0$$

$$t > 0,\ \lambda = \exp(\varepsilon^* t) \qquad\qquad (\lambda, \lambda') = \exp(\varepsilon^* t)/\exp(\varepsilon^* t')\ \text{if } t' > 0$$

Taking into account these conditions, Eq. 47 is written as:

$$P_2(\lambda, t) = c\sum_{i=1}^{3} F_i(\lambda)\mu_i(\ln \lambda/\varepsilon) - \sum_{i=1}^{3} \int_0^{\ln\lambda/z} F_i(\exp \varepsilon t)\frac{d[(\mu_i(t - t'))]}{dt'}\, dt' \qquad \textbf{(49)}$$

in which the first term corresponds to the pure relaxation.

To solve this equation, a program was written in our group by Zaddi (39).

Also, the program can be used to take into consideration the assumptions of self-consistent treatment in which the function $g(t/\tau_B)$, given by Eq. 30, is replaced by $g'(t/\tau_B)$ where:

$$g'(t/\tau_B) = 1 + (\alpha(\lambda) - 1)\mu_B(t)\mu'_B(t) \qquad (50)$$

$$\mu'_B(t) = \exp(-0.5 \times t/\tau_B) \qquad (51)$$

and, in the reptation stage, $\mu_C(t)$ becomes $\mu_C^{1+\gamma}(t)$ with $1 \leq \gamma \leq 1.3$. The program listing is given in Appendix 1.

In the study of the orientation of a polydisperse sample, the question arises concerning what is the correct molecular weight to use in Eqs. 37 and 38. For nearly monodisperse samples, the characterization of the relaxation processes can be performed using either the number-average molecular weight or weight-average molecular weight. For the case of a polydisperse sample, the choice is not obvious. Since the first relaxation process does not depend on the molecular weight, if an estimation of τ_A and τ_B was possible, one could evaluate the number of entanglements for the case of a polydisperse sample. The self-consistent treatment (20, 25) suggests that the chains do not relax independently of each other; the longer chains relax more quickly in an environment of short chains than in their pure melt state. One possible explanation is that the longer chains are not fully entangled, decreasing the number of entanglements, and if the discussion is restricted to the second relaxation process, this leads to a smaller value of τ_B. The shorter chains, in an environment of long chains, relax more slowly than in their pure melt state since their behaviour cannot be independent from that of the tube formed by the other chains.

In order to explain the relationship between τ_A and τ_B for the case of a polydisperse sample, we propose here a relationship that takes into account that each chain contributes in additive fashion to the orientation. Under this assumption, Eq. 37 can be written as:

$$\tau_{Bi} = 2\tau_A \left(M_i / M_e \right)^2 \qquad (52)$$

where τ_{Bi} is the second relaxation time for a chain of molecular weight M_i. For a polydisperse sample, an average number of entanglements is defined, to which corresponds a number-average second relaxation time τ_{BN}:

$$\tau_{BN} = \sum N_i \tau_{Bi} / \sum N_i \qquad (53)$$

where N_i is the number of chains with molecular weight M_i. From Eqs. 52 and 53, the number-average relaxation time can be written as:

$$\tau_{BN} = 2\tau_A / M_e^2 \sum N_i M_i^2 / \sum N_i \qquad (54)$$

which can be rewritten as:

$$\tau_{BN} = 2\tau_A \left(M_w M_N \right) / M_e^2 \qquad (55)$$

For a monodisperse sample Eq. 55 reduces to Eq. 37 since $M_n = M_w$, where Mn is number-average molecular weight, Mw is weight-average molecular weight.

Using the same assumptions, it is also possible to define a number-average third relaxation time, given by:

$$\tau_{CN} = 6\tau_A \left(M_W M_N M_Z \right) / M_e^3 \tag{56}$$

where Mz is Z-average molecular weight.

For the case of a monodisperse sample Eq. 56 reduces to Eq. 38.

In Figs. 18 - 22, the simulated orientation curves are compared with the experimental points at five different temperatures and four different strain rates. In the process of simulation, the assumptions of self-consistent treatment have not been considered. In order to obtain the simulation curves, it was recognized that the adjustable parameters, c, τ_A, τ_B and τ_C in Eq. 49 are not unique for a given set of experimental data, and must be reduced. It is possible to use two adjustable parameters, τ_A and c only, at temperatures where $\mu_B(t)$ and $\mu_C(t)$ can be approximated to be 1, meaning that, at these particular temperatures, the second and third relaxation processes do not influence the orientation results.

At the end of the first relaxation process, the slip network is temporarily at equilibrium and the classical expression, derived from the rubber elasticity theory, is given by Eq. 33. Since from the orientation relaxation curves, using Eq. 33, one can calculate the value of n_K, it is possible to obtain at the same time, the value of c with Eq. 40. In a previous publication from our laboratory (5), it was reported that n = 33 for PS, and, consequently, c = 0.018. Fig. 18 presents the simulated orientation curves for four different strain rates at 114°C.

Figure 18:

Experimental results and simulated orientation curves for PS
at the indicated strain rates and 114°C (Tg + 10°C) for
$\tau_A = 30$ s and c = 0.018
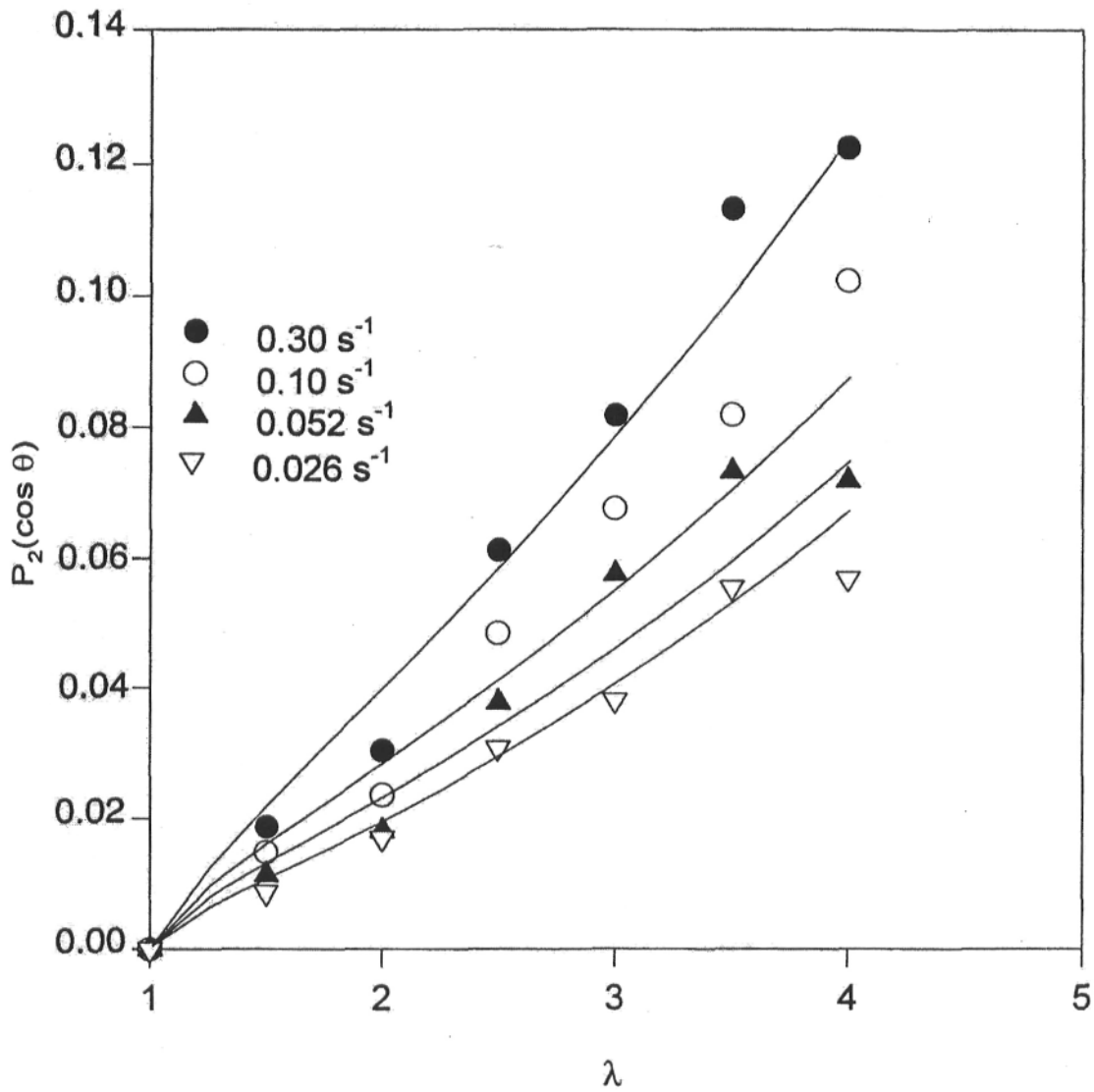
Figure 19:

Experimental results and simulated orientation curves for PS

at the indicated strain rates and 119°C (Tg + 15°C) for

$\tau_A = 5.7$ s and $\tau_B = 1140$ s
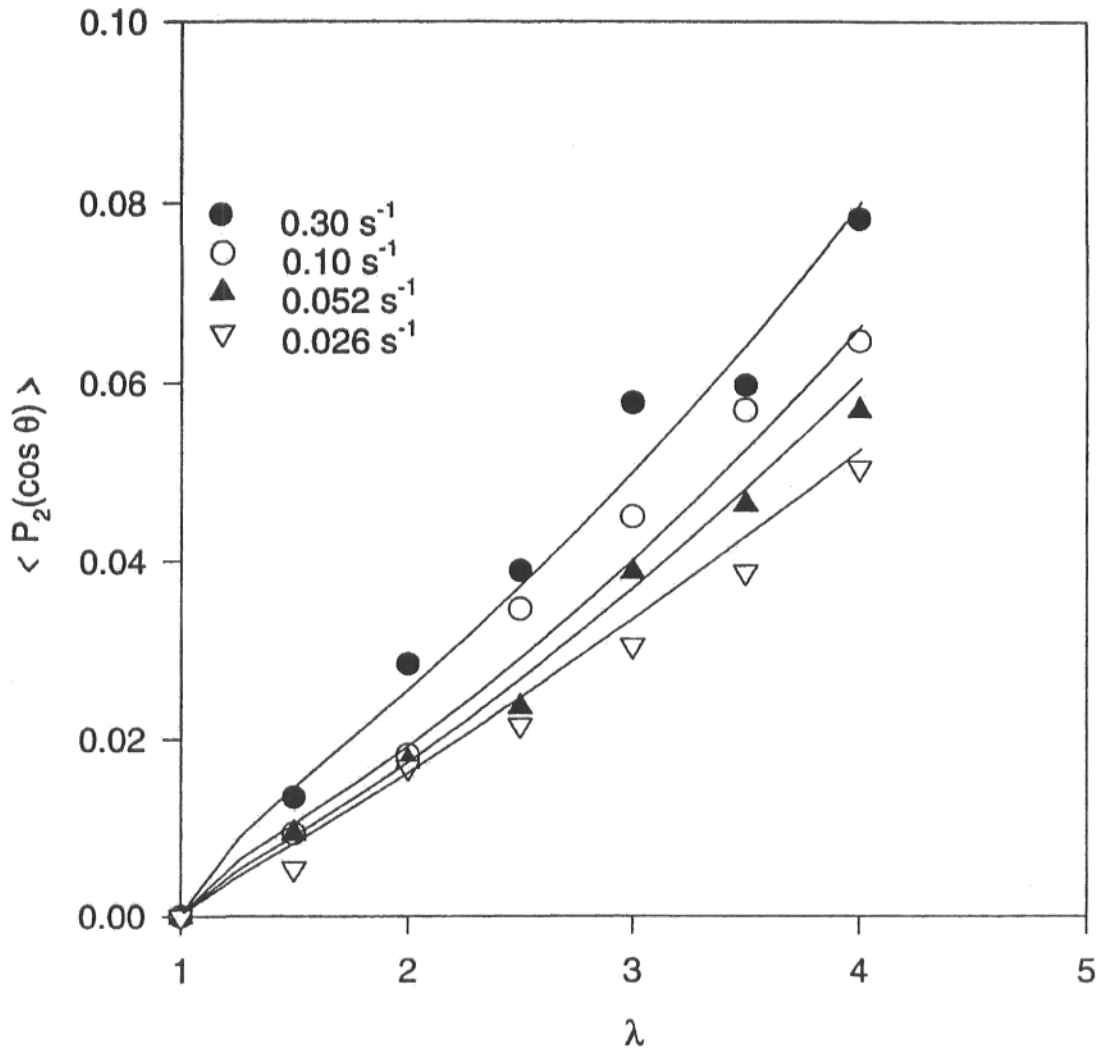
Figure 20:

Experimental results and simulated orientation curves for PS
at the indicated strain rates and 124°C (Tg + 20°C) for
$\tau_A = 1.36$ s and $\tau_B = 272$ s
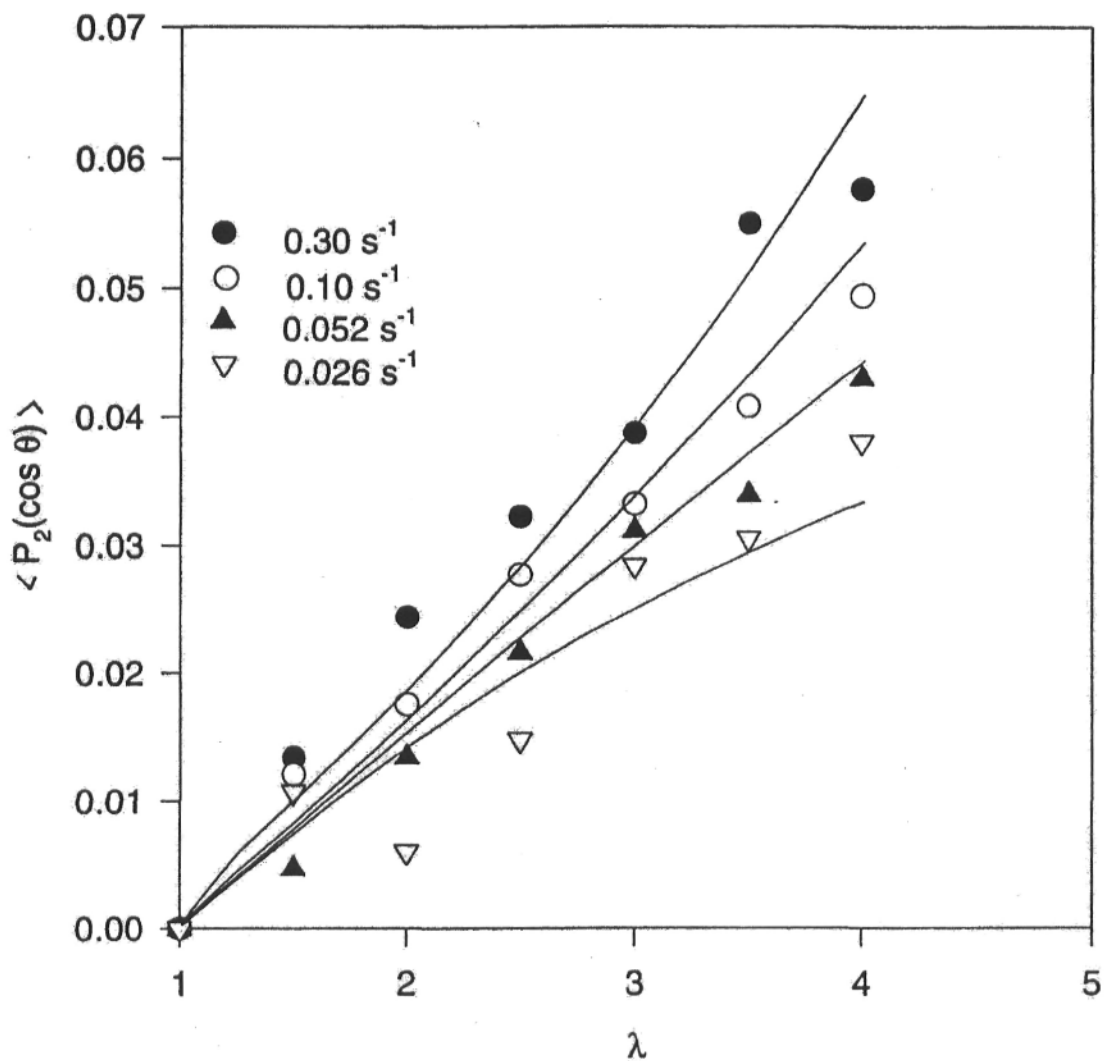
Figure 21:

Experimental results and simulated orientation curves for PS at the
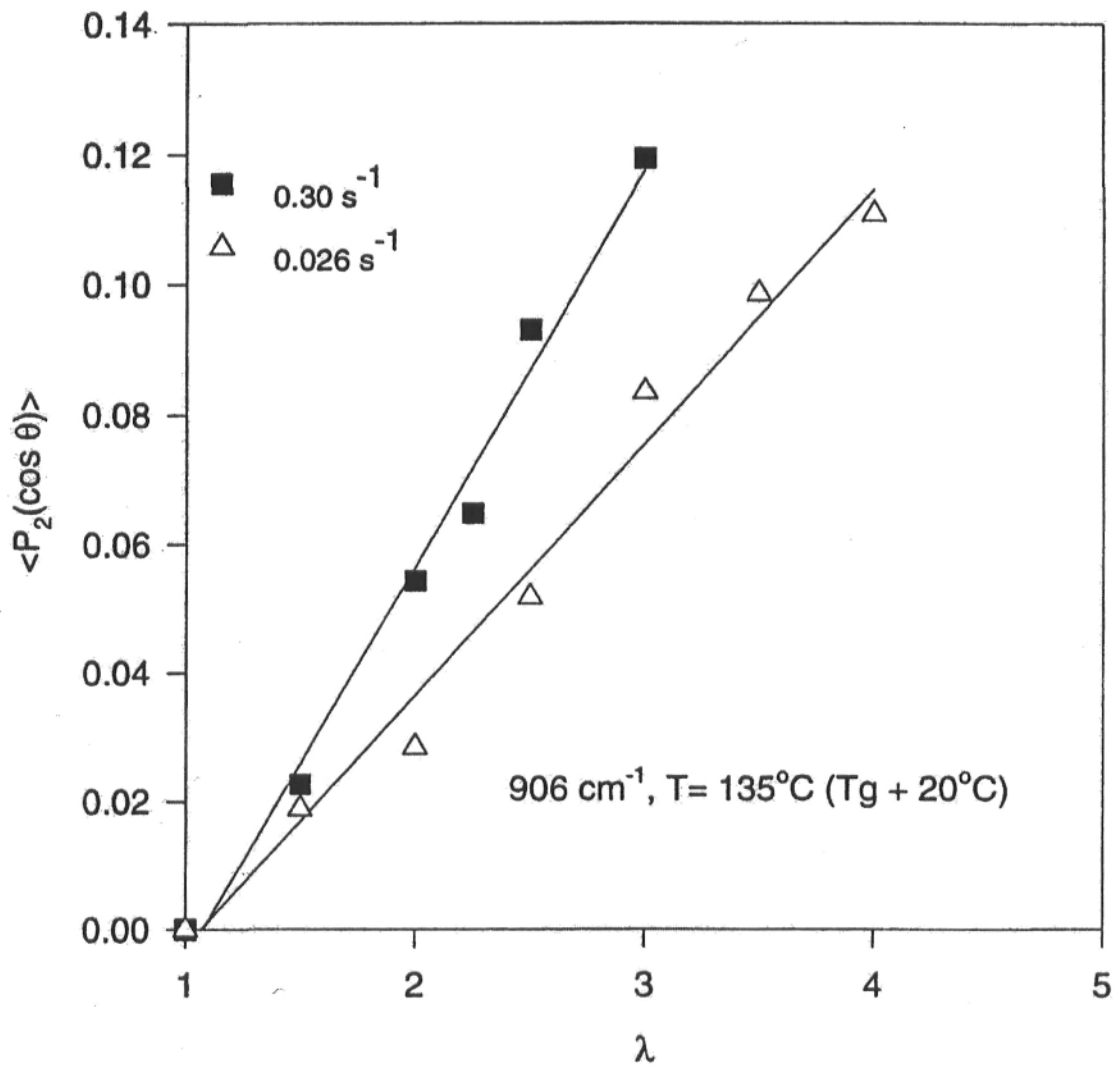indicated strain rates and 129°C (Tg + 25°C) for $\tau_A = 0.38$ s and $\tau_B = 76$ s
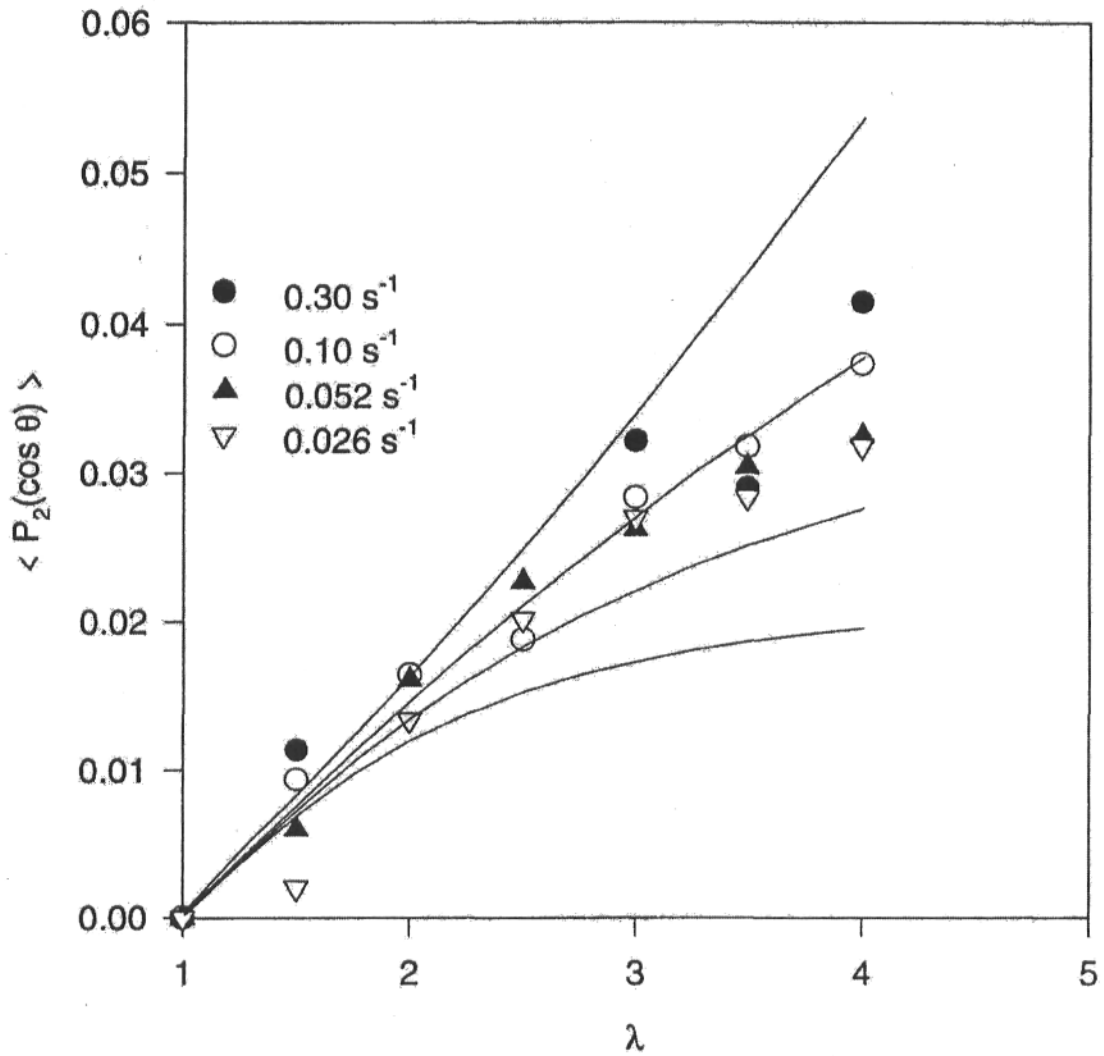
Figure 22:

Experimental results and simulated orientation curves for PS
at the indicated strain rates and 134°C (Tg + 30°C) for
$\tau_A = 0.13$ s and $\tau_B = 26$ s

For this temperature, it was considered that the second and the third relaxation processes do not influence the orientation values for the experimental times involved. As can be seen from Fig. 18, the first relaxation time used in the simulation at 114°C is 30 s, a value which is consistent with the literature data reported for this temperature (34), namely that τ_A may have values between 5.7 and 78 s. It is important to note that the values of the relaxation times are not dependent on the strain rate, as seen from Eqs. 17-19, and τ_A was chosen in such a way that the simulated curves for four different strain rates superpose simultaneously on the experimental points presented in Fig. 3.

In order to verify the assumption that, at this temperature, the second relaxation process does not influence the orientation results, second relaxation time τ_B values between 3000 and 18000 s were tested. These values correspond to a variation in the number of entanglements between 7 and 16. The slopes of the simulated orientation curves were unaffected. These limiting values for τ_B were chosen considering that the number of entanglements N_e used in Eq. 37 can be calculated as $M_n/M_e = 7$ or $M_w/M_e = 16$ since $M_e = 18,000$ for PS (34). This proves that at 114°C, for the experimental times involved, the assumption that only the first relaxation process occurs is correct.

Knowing the value of τ_A for a given temperature gives the possibility to calculate the first relaxation time for other temperatures, using the WLF coefficients, for a reference temperature T_1:

$$\tau_A(T) = \tau_A(114)*a(T/T_1)/a(114/T_1) \tag{57}$$

where the shift factors are calculated using Eq. 25. In Table 2, the first relaxation times, at different temperatures, are calculated with Eq. 57 for a reference temperature $T_1 = 120°C$. It is observed that, at more elevated temperatures, the

relaxation times have lower values, and the second and the third relaxation processes have more influence as the temperature increases.

In Figure 19, for a temperature of 119°C, the influence of the second relaxation process was taken into account in order to have a correct fit. Since c is invariable as a function of temperature, and τ_A has been calculated with Eq. 57 and is now fixed, and considering that $\mu_C(t) = 1$, it is possible to fit the set of experimental points with only one adjustable parameter, τ_B. In the program presented in Appendix 1, the values of τ_B have been adjusted by modifying the value of N_0/N_e, which allows maintaining τ_A constant. The best fit was found for a value of $\tau_B = 1140$ s, which corresponds to a value of $N_0/N_e = 10$. In order to verify the assumption that the third relaxation process does not influence the orientation values at 119°C, the simulation was performed for values of τ_B between 2×10^4 and 6×10^4 s, for τ_A and τ_B having constant values. These values correspond to the limit cases where, in Eq. 38, either M_n, or M_w, replaces M_i. The slopes of the simulated curves were again unmodified, showing that at 119°C, for the experimental times involved, the assumption that the third relaxation process does not influence the orientation values is correct.

If we consider the proposed relationship between τ_A and τ_B, presented by Eq. 55, it is observed that for $M_w = 278,000$, $M_n = 119,000$, and $M_e = 18,000$ (34), the number-average of entanglements is $M_w M_n / M_e^2 = 10.1$. At 114°C, $\tau_A = 30$ s, as obtained from the simulations presented in Fig. 18. Using Eq. 55, the number-average second relaxation time can be calculated, giving $\tau_{BN} = 6126$ s. This value is very close to that presented in Table 2, where at 114°C, $\tau_B = 6000$ s. This result indicates that the proposed Eq. 55 describes adequately the relation between the first and second relaxation times for the polydisperse sample studied.

54

Consequently, for 114°C, 124°C, 129°C and 134°C, the second relaxation times have been calculated using the value of τ_B obtained for 119°C with an equation analogous to Eq. 57, for a reference temperature of T_1= 120°C. The calculated second relaxation times are presented in Table 2.

Table 2: Relaxation times τ_A and τ_B for a polydisperse sample of PS at different temperatures.

Temperature (°C)	τ_A (s)	τ_B (s)
114 (Tg+10)	30	6000
119 (Tg+15)	5.7	1140
124 (Tg+20)	1.36	272
129 (Tg+25)	0.38	76
134 (Tg+30)	0.13	26

Using the calculated sets of relaxation times τ_A and τ_B, it was thus possible to simulate the orientation curves for 124°C, 129°C and 134°C. As seen in Figures 20, 21 and 22 the fitting is satisfactory for 124°C and 129°C. However, at 134°C, the theoretical curves show deviations for higher draw ratios, especially for $\varepsilon = 0.3$ s^{-1} and for $\varepsilon = 0.026$ s^{-1}.

The third relaxation process does not seem to influence the orientation results, even for the smallest strain rate at 134°C. Increasing the theoretical value of τ_C calculated with Eq. 38 from 780 s to any other higher value did not modify the slopes of the simulated orientation curves. The reptation process is very

complex, and the set of experimental results does not allow making any estimation of the third relaxation time.

The calculated set of relaxation times (τ_A and τ_B) used to simulate the orientation curves was used to simulate the relaxation curve at 114°C for the same polydisperse sample of PS. The results are given in Fig. 23, where the simulated relaxation curve for $\tau_A = 30$ s, $\tau_B = 6000$ s and $c = 0.018$ is compared with the experimental points. In this experiment, the sample was uniaxially stretched at a draw ratio $\lambda = 2.5$ and a strain rate of $\varepsilon = 0.3$ s^{-1}, maintained in the stretching device at the temperature of stretching for different intervals of time, and then quenched to room temperature. Besides the relaxation curve, Figure 23 presents the simulated orientation curve for a strain rate $\varepsilon = 0.3$ s^{-1} and a draw ratio $\lambda = 2.5$. Both curves were drawn with the same set of c, τ_A, τ_B, and τ_C parameters. In order to simultaneously simulate the orientation and the relaxation of orientation curves, a modified form of Eq. 29 was used, since there are limitations in using this equation as is. For instance, for very short times, and more specifically for $t = 0$ when $\mu_B(t) = \mu_C(t) = 1$, the value of $\mu_A(t)$ from Eq. 34 depends on the number of the exponential terms used for calculation. For instance, at $t = 0$ for $\lambda = 4$ and $c = 0.018$, the calculated value for P_2 is 0.36 when $\mu_A(t)$ is calculated with three exponential terms and 0.46 when $\mu_A(t)$ is calculated with four exponential terms ($\mu_A(t)$ increases with the number of exponential terms). As a function of time, the value of P_2 decreases very quickly and, after a short interval of time, there is almost no difference in P_2 values if $\mu_A(t)$ is calculated with three or more exponential terms. When simultaneously simulating the orientation and relaxation of orientation curve, the relaxation is considered to start at a time t_0 (t_0 is the stretching time), so the highest value of orientation, corresponds with $P_2(t_0)$, the first value of the relaxation curve. If in Eq. 29 we consider $t = t_0$, then:

$$P_2(t_0) = P_2^{network} \gamma \alpha^2 (\lambda) * \mu_A(t_0) g^2 (t_0/\tau_B) \mu_C(t_0) \qquad (58)$$

then for t= t_0+t':

$$P_2(t_0 + t') = P_2^{network} \gamma \alpha^2 (\lambda) * \mu_A(t_0 + t') g^2 (t_0 + t'/\tau_B) \mu_C(t_0 + t') \qquad (58')$$

From Eqs. 58 and 58' it can be deduced that:

$$P_2(t_0 + t') = P_2(t_0) * \frac{\mu_A(t_0 + t') g^2 (t_0 + t'/\tau_B) \mu_C(t_0 + t')}{\mu_A(t_0) g^2 (t_0/\tau_B) \mu_C(t_0)} \qquad (59)$$

Eq. 59 reduces to Eq 29 for $t_0 = 0$. In Figure 23 the relaxation curve is a plot of $P_2(t_0 + t')$ versus t', where t' ≥ 0. The relaxation curve seems to fit the experimental points adequately. For this case, $t_0 = 3.06$ s. In the same figure the simulated relaxation curve is presented for a value of $t_0 = 0$, which corresponds to the unmodified form of Eq. 29. This shows that, for the same set of parameters, the simulated orientation values are higher than the experimental values at the beginning of the relaxation process, but exhibit the same behaviour for higher values of time.

The above simulation procedures were applied (in more limited fashion because fewer experimental data are available) to PS-SSA. In Figure 24, the orientation behaviour of PS-SSA (4.7%) was simulated for T = Tg +15°C.
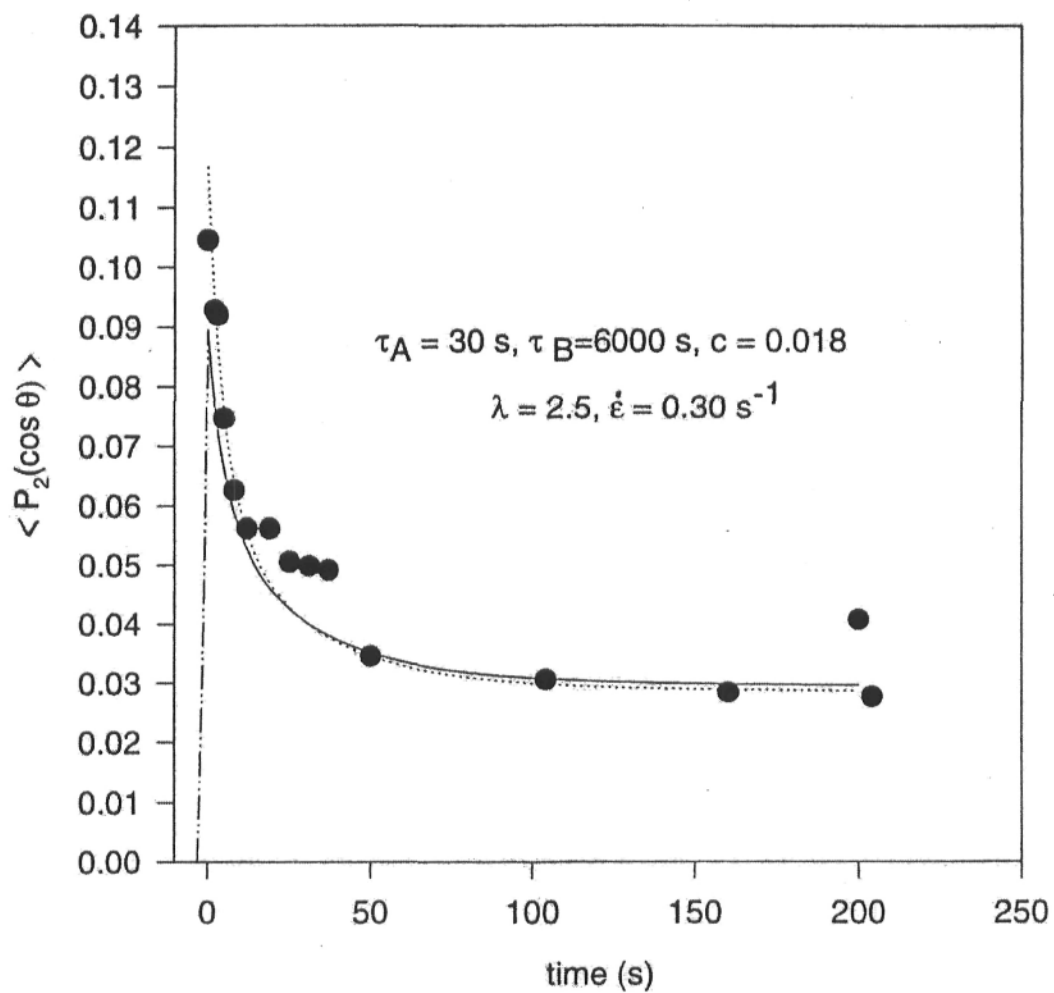
Figure 23:

Experimental results, simulated orientation curves and simulated
relaxation behaviour of PS at T=114°C (Tg+10°C)

●   experimental points

—··—··—··   the simulated orientation curve from Figure 18

·················   the relaxation behaviour for $t_0 = 0$

————   the relaxation behaviour for $t_0 = 3.06$ s
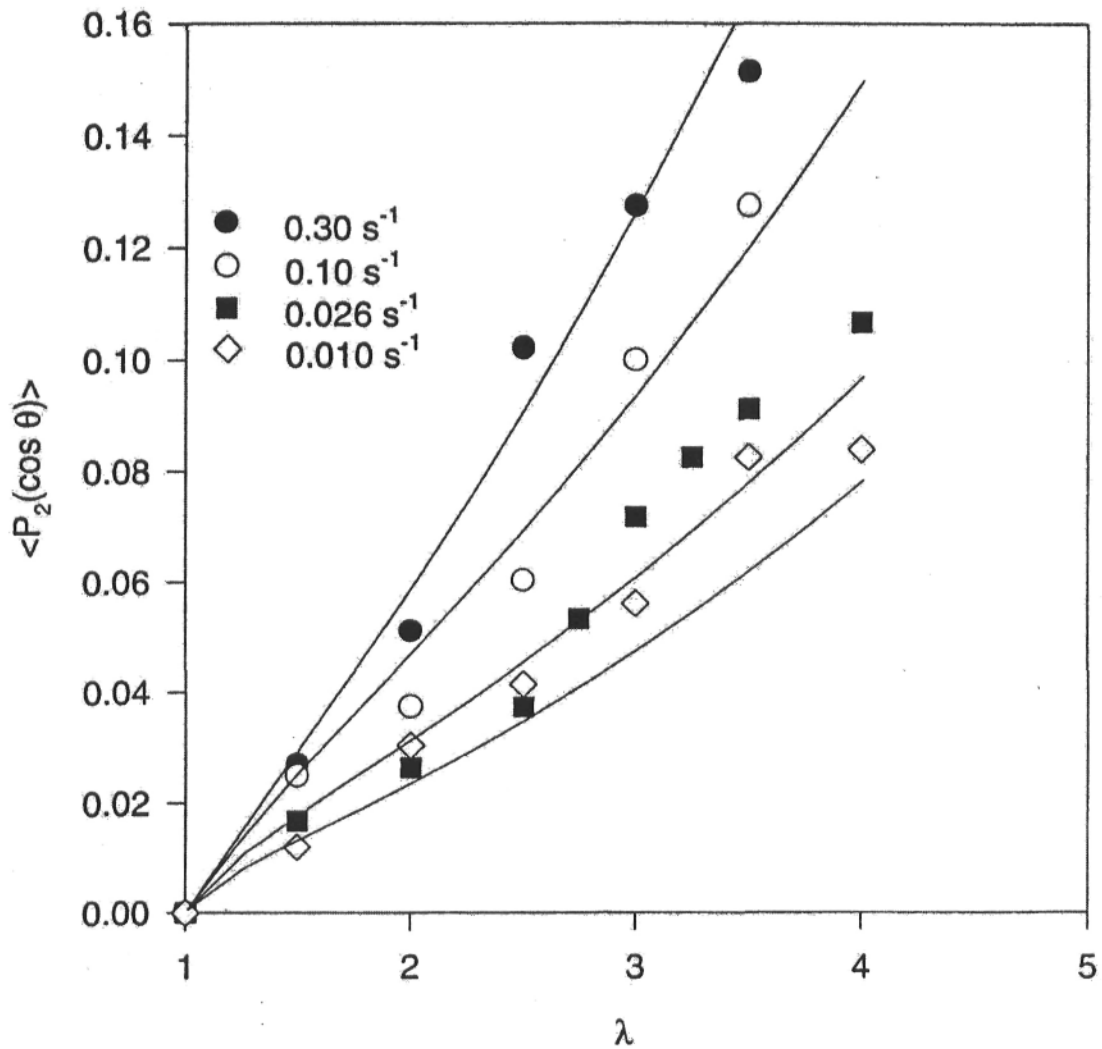
Figure 24:

Experimental results and simulated orientation curves for PS-SSA 4.7 %

at the indicated strain rates, 127°C (Tg + 15°C) and λ = 2.5 for

τ_A = 25 s, τ_B = 11250 s and τ_C = 5 x10^5 s

The simulation was performed at four different strain rates, using $N_0/N_e = 10$, as obtained from the simulation curves of PS, keeping the same value $c = 0.018$ as for PS. The best fit was considered to correspond to $\tau_A = 25$ s and $\tau_B = 5000$ s. The correctness of these values was verified by using them to simulate a relaxation curve and comparing with the experimental points using Eq. 59. The results are presented in Fig 25. In the same figure, as in the case of PS, the simulation curve for $t_0 = 0$, that corresponds to Eq. 29, is also given.

Comparing the values of the relaxation time of sulphonated PS and PS at $T = T_g+15°C$, it is observed that the copolymer exhibits a much higher value of the relaxation time (25 s) than PS (5.7 s). As seen from Eq. 17, the first relaxation time depends on the bond length of the real chain, on the number of repeat units between entanglements or effective crosslinks, and on the friction coefficient. If it is supposed that the first two parameters are almost unmodified, then it can be considered that the higher orientation values of sulphonated PS compared to PS is due to the higher values for the friction coefficient.

If the SSA interactions act like effective crosslinks, then the value of c should be different from that used in the simulation. Also, the molecular weight between entanglements should be different from that of PS. That can also modify the values of the relaxation times to a certain extent. In order to have more information about the crosslinking effects, further investigations are necessary.

60
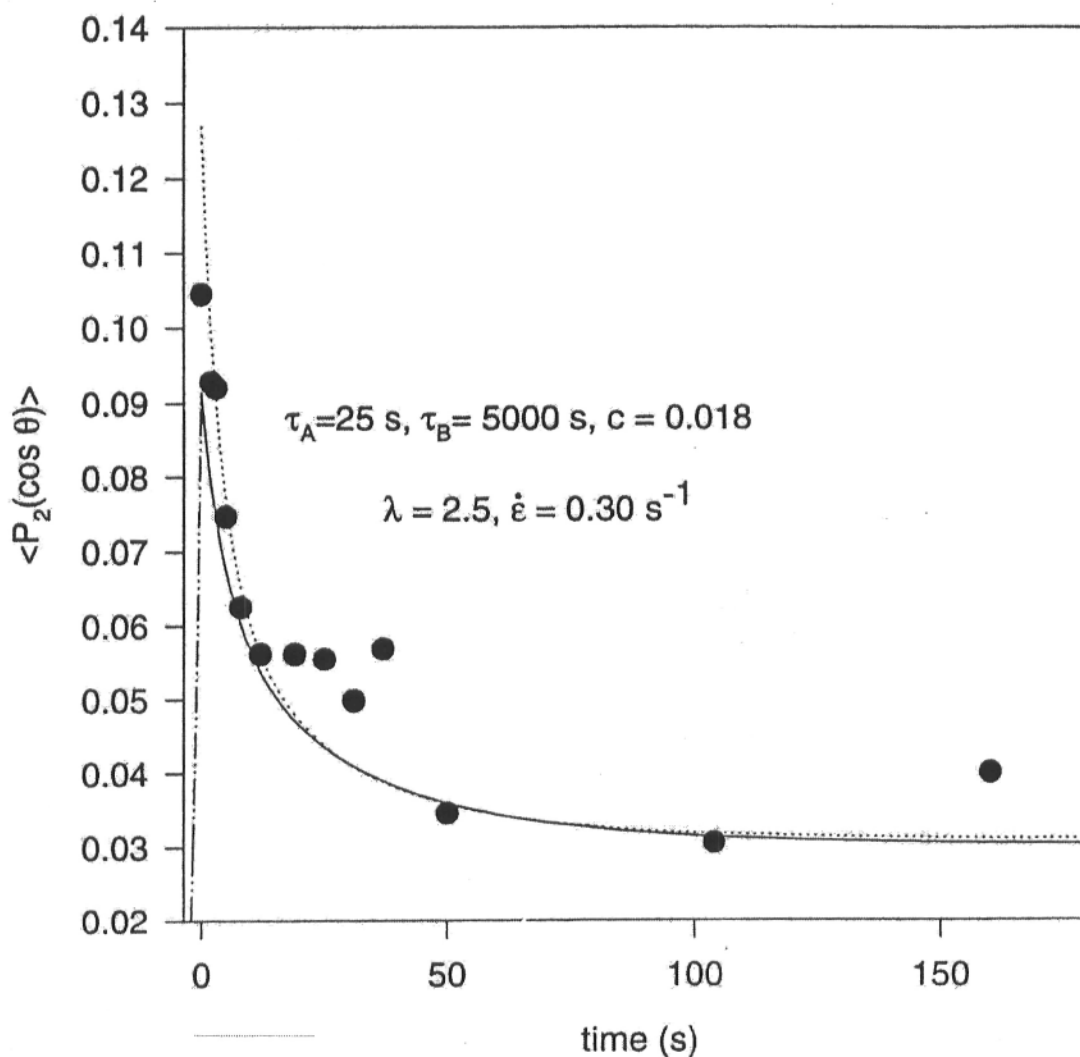
Figure 25:

Experimental results, simulated orientation curves and simulated
relaxation behaviour of PS-SSA 4.7 % at T=127°C (Tg+15°C)

●   experimental points

—··—··—··   the simulated orientation curve from Figure 24
           the relaxation behaviour for $t_0 = 0$

————   the relaxation behaviour for $t_0 = 3.06$ s

4. Conclusions and Perspective

The general objective of this mémoire was to study the molecular orientation of polystyrene and some polystyrene-based systems, poly(styrene-co-styrene sulphonic acid (4.7%), and PS-SSA 5.0% with poly(styrene-co-4-vinyl-pyridine) 4.5%.

The orientation of polystyrene was studied at different temperatures and different strain rates, from which it was possible to draw an orientation-relaxation master curve. This behavior shows that the principle of time-temperature superposition applies to infrared measurements of samples that are stretched uniaxially at exponential stretching velocities, as previously shown for linear stretching velocities. The orientation-relaxation master curve also provides a general picture of the orientation behavior for a given polymer.

The orientation of the PS-SSA (4.7%) blend, studied for the 1028 cm^{-1} band, was higher than that of PS, using Tg as the reference temperature. This behaviour is explained taking into account the hydrogen-bonding interactions between sulphonic acid groups. The orientation of PS-SSA (4.7%) was also studied using birefringence, which is a complementary technique of infrared dichroism.

The study of a blend of PS-SSA 4.7% with poly(styrene-co-4-vinyl-pyridine) (4.5%) showed that the orientation values are much higher for ionomer blends in comparison with those of their acid precursors or parent homopolymers. As previously observed (10), the ion-ion interactions exert a clear influence on the orientation achieved.

A theoretical analysis based on the Doi-Edwards model permitted the determination of a set of characteristic relaxation times for PS and for PS-SSA (4.7%), and the simulation of orientation and relaxation curves. If the values for c and τ_A are established with sufficient precision for a temperature where the other relaxation processes do not occur, then the simulations for higher temperatures allow finding the values for the second relaxation time. In the case of a polydisperse sample, it was shown that, for the second relaxation time, the molecular weight cannot be replaced simply by the number-average molecular weight or by the weight-average molecular weight. A number-average second relaxation time was defined from the assumption that, in polydisperse samples, the longer molecules are not fully entangled and therefore they have a shorter second relaxation time in comparison with the monodisperse samples. On the other hand, the shorter molecules are not able to relax independently from the surrounding molecules therefore have a longer second relaxation time in comparison with monodisperse samples. It was shown that the number-average second relaxation time depends on the product between the number-average molecular weight and the weight-average molecular weight. The experimental results are in concordance with this theoretical prediction.

Since the completion of this work in 1995, other studies of orientation and orientation relaxation have been published. Most closely related to the present work are investigations using linear dichroism of ionomer blends, in particular blends of ionomers with small molecules (41-43) and blends of two complementary ionomers (43, 44). Orientation measurements obtained by infrared linear dichroism of ionomer blends of poly[ethyl acrylate-co-(4-vinylpyridine)] (PEA-VP) with of poly[styrene-co-(styrenesulfonic acid)] (PS-SSA) (43, 44) showed, for blends with similar counit contents (symmetric blends), that the segmental orientation of both the polystyrene and poly(ethyl acrylate)

segments increases with ion content, a direct result of the effective ionic cross-links. However, the orientation of polystyrene segments in asymmetric blends is much higher than in symmetric blends. The difference in behaviour of symmetric and asymmetric blends is explained considering that the orientation of symmetric blends is affected by a plasticization effect from the poly(ethyl acrylate) segments, attributed to relaxation coupling between the dissimilar chains during stretching.

In recent years, infrared dichroism (IRLD) has been coupled with polarization modulation (PM), in which a fast change of the state of polarization of the incident infrared light beam is produced by a photoelastic modulator (45, 46). The use of PM-IRLD permits the study of orientation and relaxation kinetics of different blend components in real time, thus minimizing instrumental and sample fluctuations. This greatly reduces the experimental error that is encountered due to the time the sample needs to cool down from the stretching temperature in the stretch-freeze experiments. Most importantly, the relaxation behavior can be studied from very small to large intervals of times using the same sample. This permits the simultaneous study of different relaxation processes.

For poly(tetramethylene oxide) (PTMO) zwitterionomers of different PTMO segment lengths, the orientation and relaxation behaviour was studied, using both infrared linear dichroism (47) and PM-IRLD (48). Since strong ionic interactions lead to the formation of a biphasic morphology, a comparison between the orientation and relaxation behaviour of PTMO segments (low Tg phase) and the sulfonate units (high Tg phase) was performed. The magnitude of the orientation function of PTMO chains is observed to decrease with temperature, and it was shown that the ionic aggregates do not behave as permanent cross-link points. The results obtained also revealed that the hard zwitterionic domains show a reversal in their orientation direction during the drawing process. This phenomenon is explained by a progressive disruption of the ionic domains in

64

response to the applied stress and deformation. In addition, stress-induced crystallization of the PTMO chains could be observed for one of the studied systems during relaxation over a long period of time.

Orientation studies of phase-separated PS/PVME blends using infrared linear dichroism and birefringence showed that the orientation of PS is higher in the immiscible than in the miscible blends when the Tg of the miscible blend is taken as the reference temperature (49). The orientation and relaxation behaviour of miscible PS/PVME blends and the effect of thermal history on the orientation and relaxation behavior of miscible and phase-separated PS/PVME blends was subsequently studied by PM-IRLD (50-52). The orientation and relaxation behaviour of the PS and PVME chains was explained considering the morphology of the sample including the presence of concentration fluctuations in miscible blends and the effect of the local environment on the rigidity of the chains.

PM-IRLD and birefringence were also used to directly measure PS relaxation curves following a step of deformation in different conditions of temperature, draw rate and for different molecular weights (53, 54). An excellent correlation was obtained between the two techniques. The quantitative analysis of relaxation curves was carried out using a three-term exponential decay function. The first relaxation time showed a good correlation with previous results (20, 25). The values obtained for the second relaxation could not be interpreted by the Doi-Edwards model, and was attributed to the existence of a difference in the friction coefficient between the ends and middle of the chain.

IRLD was used as well to study the orientation of poly(vinylphenol (PVPh) and PVPh - poly(methyl methacrylate) (PMMA) blends (55). It was observed that PMMA orientation is larger than that of PVPh, but decreases with increasing PVPh composition. The orientation of the two components is higher in blends that

are richer in PMMA. The increase in the orientation of PVPh chains in these blends was attributed to a larger entanglement density. On the other hand, in rich PVPh blends the PMMA chains are rigidified, thus decreasing their entanglement density and consequently their orientation.

The non-negligible poly(ethylene oxide) (PEO) orientation in the PVPh/PEO blends (56) was attributed to strong hydrogen bonds between the dissimilar chains. For a composition of 30 wt % PEO, the PEO orientation goes through a maximum, while PVPh just begins to orient. This maximum, corresponding to around 1:1 mole ratio of interacting units is considered to be related to a maximum in the number of hydrogen bond interactions in this system. A maximum in the orientation values was also observed for PVPh/PVME blends (57), for a composition close to a 1:1 mole ratio of interacting units. This behaviour was explained in terms of cooperativity of deformation and relaxation between the blend components. Molecular modeling simulations were also performed for the uniaxial deformation of PVPh (58) and PVPh/PVME blends (59).

Molecular orientation and relaxation of conformers of poly (ethylene terephthalate) (PET) after uniaxial deformation above the glass transition temperature were also investigated using PM-IRLD (60, 61). It was found that the trans conformers orient much more that the gauche conformers, whereas their relaxation rates are comparable. A re-orientation phenomenon was associated with the crystallization of the polymer. Rouse relaxation times were estimated from birefringence relaxation data (62). PET molecular parameters, such as molecular weight between entanglements and friction coefficient, were calculated from rheological master curves. The reptation and retraction time were calculated using the scaling laws proposed by Doi and Edwards.

The work described in this mémoire was intended to be a basis for subsequent Ph.D. studies. It would have been interesting to follow up on ref. 44, and use the PM-IRLD technique to learn how the ion interactions in ionomer blends, particularly in symmetrical and asymmetrical blends of poly[(ethyl acrylate)-*co*-(4-vinyl pyridine)] with poly[styrene-*co*-(styrenesulfonic acid)], affect orientation relaxation. In connection with this, the following questions can be adressed. How is the orientation relaxation of dissimilar chains compare in symmetric and asymmetric blends? How the orientation of dissimilar chains is influenced by very low and very high PS content? Is it intrinsic orientation that is affected through effective crosslinks? Can we determine the number of effective crosslinks? Is the number of effective crosslinks influenced by temperature or other factors?

These questions might be answered with the more precise orientation measurements afforded by the PM-IRLD technique, the experimental determination of orientation relaxation behavior using this technique, and simulation of the behaviour based on Doi-Edwards concepts.

References:

1. Ward, I. M., *Structure and Properties of Oriented Polymers,* Applied Science Publ., London, 1975.

2. Lefebvre, D., Jasse, B., Monnerie, L., *Polymer,* 1981, 22, 1616.

3. Lefebvre, D., Jasse, B., Monnerie, L., *Polymer,* 1982, 23, 706.

4. Lefebvre, D., Jasse, B., Monnerie, L., *Polymer,* 1984, 25, 318.

5. Zhao, Y., Prud'homme, R. E., Bazuin, C. G., *Macromolecules,* 1991, 24, 1261.

6. Abtal, E., Prud'homme, R. E., *Macromolecules,* 1994, 27, 5780.

7. Abtal, E., Prud'homme, R. E., *Polymer,* 1993, 34, 4661.

8. Zhao, Y. C., Bazuin, C. G., Prud'homme, R. E., *Macromolecules,* 1989, 22, 3788.

9. Smith. P., *Ph.D. Thesis,* Dept. of Chemistry, McGill University, Canada, 1985.

10. Bazuin, C. G., Fan, X. D., Lepilleur, C., Prud'homme, R. E., *Macromolecules,* 1995, 28, 897.

11. Fan, X. D., Bazuin, C. G., *Macromolecules,* 1993, 26, 2508.

12. de Gennes, P.G., *J. Chem. Phys.,* 1971, 55, 572.

13. Wool, R. P., *Macromolecules,* 1993, 26, 1564.

14. Wool, R. P., *Macromolecules,* 1986, 19, 1963.

15. Wool, R. P., *Macromolecules,* 1987, 20, 1924.

16. Doi, M., Edwards, S. F., *J. Chem. Soc. Faraday Trans. II,* 1978, 74, 1789.

17. Doi, M., Edwards, S. F., *J. Chem. Soc. Faraday Trans. II,* 1978, 74, 1802.

18. Doi, M., Edwards, S. F., *J. Chem. Soc. Faraday Trans. II,* 1978, 74, 1818.

19. Doi, *M., J. Polym. Sci. Polym. Phys. Ed.,* 1980, 18, 1005.

20. Viovy, J. L., *J. Polym. Sci. Polym. Phys. Ed.,* 1981, 19, 265.

21. Doi, M., *J. Polym. Sci. Polym. Lett. Ed.,* 1985, 23, 2423.

22. Viovy, J. L., Monnerie, L., Tassin, J. F., *J. Polym. Sci: Part B: Polym. Phys.,* 1983, 21, 2427.

23. Graessley, W. W., *Adv. Polym. Sci.,* 1982, 47, 67.

24. Kornfield, J. A., Fuller, G. G., Pearson, D. S., *Macromolecules,* 1989, 22, 1334.

25. Merrill, W. W, Tirrell, M., Tassin, J. F., Monnerie, L., *Macromolecules,* 1989, 22, 896.

26. Bower, D. T., *J. Polym. Sci. Polym. Phys. Ed.,* 1981, 19, 99-107.

27. Ingle, J. D., Crouch, S. R., *Spectrochemical Analysis,* Prentice Hall, Inc., New Jersey, 1988.

28. Buffeteau, T., Desbat, B., Pézolet, M., Turlet, J. M., *J. Chem. Phys.,* 1993, 90, 1467.

29. Stein, R. S., *J. Appl. Phys.,* 1961, 32, 1280.

30. Makowski, H. S., Lundberg, R. D., Singhal, G. H., *U.S. Patent,* 1977, 3, 870, 841.

31. Jasse, B., Koenig, J. L., *J. Polym. Sci. Polym. Phys. Ed.,* 1979, 17, 799.

32. Plazek, D. J., *J. Phys. Chem,* 1965, 69, 10.

33. Tassin, J. F., *Thèse d'État,* Univ. Paris VI, 1986.

34. Tassin, J. F., Monnerie, L., *Macromolecules,* 1988, 21, 1846.

35. Zundel, G., *Hydration and Intermolecular Interaction,* Academic Press: New York, 1969.

36. Yang, S., Sun, K., Risen, W. M., *J. Polym. Sci. Part B: Polym. Phys.,* 1990, 28, 1685.

37. Abtal, E., *Ph.D. Thesis,* Dept. of Chemistry, Université Laval, Québec, Canada, 1990.

38. Eisenberg, A., Navratil, M., *Macromolecules,* 1973, 6, 604.

39. Zaddi, E. H., *Ph.D. Thesis,* Dept. of Chemistry, Université Laval, Québec, Canada, 1997.

40. Tassin, J. F., Baschewitz, A., Moise, I. Y., Monnerie, L., *Macromolecules,* 1990, 23, 1879.

41. Fan, X. D., Bazuin, C. G., *Macromolecules*, 1995, 28, 8209.

42. Fan, X. D., Bazuin, C. G., *Macromolecules*, 1995, 28, 8216.

43. Fan, X. D., *Ph.D. Thesis,* Dept. of Chemistry, Université Laval, Québec, Canada, 1996.

44. Fan, X. D., Bazuin, C. G., *Macromolecules*, 1998, 31, 1321.

45. Buffeteau, T., Pezolet, M., *Appl. Spectrosc.*, 1996, 50, 948.

46. Pézolet, M., Pellerin, C., Prud'homme, R. E., Buffeteau, T., *Vib. Spectrosc.*, 1998, 18, 103.

47. Wang, Y., Bazuin, C. G., Pézolet, M., *Macromolecules,* 2001, *34,* 6344.

48. Wang, Y., Pellerin, C., Bazuin, C. G., Pézolet, M., *Macromolecules* 2005, *38,* 4377.

49. Abtal, E., Prud'homme, R.E., *Polymer*, 1996, 37, 3805.

50. Pellerin, C., *Ph.D. Thesis,* Dept. of Chemistry, Université Laval, Québec, Canada, 2002.

51. Pellerin, C., Prud'homme, R. E., Pézolet, M., *Macromolecules,* 2000, 33, 7009.

52. Pellerin, C., Prud'homme, R. E., Pézolet, M., *Polymer,* 2003, 44, 3291.

53. Messé, L., *Ph.D. Thesis,* Dept. of Chemistry, Université Laval, Québec, Canada, 1998.

54. Messé, L., Pézolet, M., Prud'homme, R. E., *Polymer,* 2001, 42, 563.

55. Li, D., Brisson, J. *Macromolecules*, 1997, 30, 8425.

56. Rinderknecht, S., Brisson, J., *Macromolecules*, 1999, *32*, 8509.

57. Gestoso, P., Brisson, J., *Polymer*, 2001, 42, 8415.

58. Gestoso, P., Brisson, J., *J. Polym. Sci, Part B: Polym. Phys.,* 2002, 14, 1601.

59. Gestoso, P., Brisson, J., *Polymer,* 2003, 44, 2321.

60. Duchesne, C., *M.Sc. Thesis*, Dept. of Chemistry, Université Laval, Québec, Canada,1999.

61. Duchesne, C., Kong, X., Brisson, J., Pézolet, M., Prud'homme R.E., *Macromolecules,* 2002, 35, 8768.

62. Oultache, K., Kong, X., Pellerin, C., Brisson, J., Pézolet, M., Prud'homme, R. E., *Polymer,* 2001, 42, 9051.

Appendix 1

This program , written by Zaddi E. H. (39), permits the simulation of the orientation curves for the case of an exponential velocity of stretching.

```
REM************************************************************************
REM                        CALCULS DE L'ORIENTATION
REM************************************************************************

Origine:
        DIM f(4), ff(4), u(4), du(4) AS DOUBLE
        DIM ua, ub, uc, ua1, ub1, ubp1, uc1 AS DOUBLE
        DIM dua1, dub1, duc1, dubp1 AS DOUBLE

        DECLARE FUNCTION asinh! (x!)

        ON KEY(1) GOSUB Cle1: KEY(1) ON
        ON KEY(2) GOSUB Cle2: KEY(2) ON
        ON KEY(10) GOSUB Cle10: KEY(10) ON

        REP$ = "A:\": NOM$ = "RESUL.ASC"                        ' Repertoire
par defaut
        ne = 16                        ' Nombre d'enchevetrements par chaine
        v = .026:  PI = 3.141592:

        SCREEN 12

Commence:
        CLS
        LINE (0, 0)-(639, 479), 9, B: LINE (3, 2)-(636, 477), 9, B
        LOCATE 2, 30: COLOR 14: PRINT "CALCUL DE L'ORIENTATION"
        LOCATE 29, 3: PRINT "F1: Début            F2: Paramètres de calcul
          F10: Sortie";


        LOCATE 5, 5: COLOR 15: PRINT "Ce programme permet le calcul de
l'orientation P2 en fonction du temps de"
        LOCATE 6, 5: PRINT "rétraction (tb), en appliquant les lois d'échelle pour
ta et tb, et en"
        LOCATE 7, 5: PRINT "connaissant ε'(1), Ns(3), N(20), τ(1), nhu'(0.5), pour
des rapports"
        LOCATE 8, 5: PRINT "d'étirement variant de 1.01 à 4.01."
```

```
        LOCATE 10, 5: COLOR 15: PRINT "Le répertoire par défaut est b:\"
        LOCATE 11, 5: PRINT "Si vous voulez un autre répertoire, écrivez-le avec
votre nom de fichier"
        LOCATE 13, 5: INPUT "Nom du fichier où aura lieu la sauvegarde : ", NO$
        IF NO$ <> "" THEN NOM$ = NO$

        B$ = LEFT$(NOM$, 2): c$ = RIGHT$(B$, 1)
        IF c$ <> ":" THEN NOM$ = REP$ + NOM$
        OPEN NOM$ FOR APPEND AS #1              'Creation du fichier de donnees

        LOCATE 16, 24: COLOR 14: PRINT "VALEURS DES PARAMETRES DE
CALCUL": COLOR 15
        LOCATE 19, 14: INPUT "tb : ", tb              ' Temps de retraction
        LOCATE 19, 57: INPUT "G0 : ", c               ' Module d'elongation

        NNN = 13

Calculs:
        ta = tb / (2 * ne ^ 2)              ' Temps de reequilibrage local
        tc = 6 * ne ^ 3 * ta                ' Temps de reptation
Tabl:
        CLS : LINE (0, 0)-(639, 479), 9, B: LINE (3, 2)-(636, 477), 9, B

        LOCATE 2, 33: PRINT "RESULTATS DES CALCULS"
        LOCATE 6, 5: PRINT USING "ta = ####.####      tb = #####.####      tc
= ######.####"; ta; tb; tc
        LOCATE 7, 5:  PRINT USING "Module d'élongation -->    G0 = ####.####
"; c        ' Reperes
        LINE (20, 130)-(619, 170), 15, B: LINE (22, 132)-(617, 168), 15, B
        LINE (20, 170)-(619, 420), 15, B: LINE (22, 170)-(617, 418), 15, B

        LOCATE 10, 7: PRINT "         n            R            Z
<P2> "

        PRINT #1, "ta = "; ta              ' Incription des temps et de G0 dans
        PRINT #1, "tb = "; tb              ' dans le fichier de donnees
        PRINT #1, "tc = "; tc
        PRINT #1, "c = "; c
        PRINT #1, ""

FOR n = 1.01 TO 4.01 STEP .25              ' Boucle de n (Taux d'etirement)

                                           ' Calcul de R
        R = 0                              ' Mise a zero

        x = n ^ 3 - 1: x = SQR(x)
```

```basic
t = LOG(n) / v

ua = 1 + EXP(-t / ta) + EXP(-4 * t / ta) + EXP(-9 * t / ta)
ub = (8 / PI ^ 2) * (EXP(-t / tb) + (1 / 9) * EXP(-9 * t / tb))
uc = (8 / (PI ^ 2)) * (EXP(-t / tc) + (1 / 9) * EXP(-9 * t / tc))
ubp = EXP(-t * .5 / tb)

u(1) = ua * uc ^ 2
u(2) = u(1) * ub * ubp
u(3) = u(2) * ub * ubp

a = 1 / 2 * (n + asinh(x) / (x * SQR(n)))
a1 = a: Y = n
GOSUB CalcF

FOR i = 1 TO 3                    ' Calcul de R pour un 'n' donne
    R = R + c * f(i) * u(i)
NEXT i

                                 ' Calcul de Z
Z = 0                            ' Mise a zero

' Calcul de l'integrale (calcul de l'aire par exces)

FOR i = 1 TO 3
    ff(i) = 0                    ' Mise a zero de l'integrale (ff)
    K = (LOG(n)) / v             ' Borne superieure de l'integrale
    pas = K / 100                ' Precision de l'integrale
    ini = pas                    ' Debut de l'integrale

    FOR s = ini TO K STEP pas
        nn = n * EXP(-v * s)
        IF nn = n THEN GOTO Boucs         ' Ote la singularite

        ua1 = 1 + EXP(-s / ta) + EXP(-4 * s / ta) + EXP(-9 * s / ta)
        ub1 = (8 / (PI ^ 2)) * (EXP(-s / tb) + (1 / 9) * EXP(-9 * s / tb))
        uc1 = (8 / (PI ^ 2)) * (EXP(-s / tc) + (1 / 9) * EXP(-9 * s / tc))
        ubp1 = EXP(-s * .5 / tb)

        dua1 = -(1 / ta) * (EXP(-s / ta) + 4 * EXP(-4 * s / ta) + 9 * EXP(-9
* s / ta))

        dub1 = (-8 / (tb * PI ^ 2)) * (EXP(-s / tb) + EXP(-9 * s / tb))
        duc1 = (-8 / (tc * PI ^ 2)) * (EXP(-s / tc) + EXP(-9 * s / tc))
        dubp1 = (-.5 / tb) * EXP(-s * .5 / tb)

        du(1) = dua1 * uc1 ^ 2 + 2 * uc1 * duc1 * ua1
```

```basic
                du(2) = du(1) * ub1 * ubp1 + ua1 * (uc1 ^ 2) * (dub1 * ubp1 +
ub1 * dubp1)

                du(3) = du(2) * ub1 * ubp1 + ua1 * (uc1 ^ 2) * ub1 * ubp1 *
(dub1 * ubp1 + ub1 * dubp1)

                Y = n / nn
                x = (Y ^ 3 - 1): x = SQR(x)
                a1 = 1 / 2 * (Y + asinh(x) / (x * SQR(Y)))

                GOSUB CalcF

                                        ' Calcul de l'aire
                ff(i) = ff(i) + f(i) * du(i) * pas

Boucs:
        NEXT s

        Z = Z + c * ff(i)                   ' Integrale finale
    NEXT i

    P2 = R - Z                          ' Calcul de l'orientation

    LOCATE NNN, 7: PRINT USING "  #.###      ##.#####      ##.#####
##.#####      "; n; R; Z; P2;  ' Reperes
    PRINT #1, n, P2                     ' Inscription dans le fichier

    NNN = NNN + 1
NEXT n

PRINT #1, "": PRINT #1, ""
CLOSE #1
COLOR 14: LOCATE 28, 5: PRINT "FAITES 'C' POUR COMMENCER UN
NOUVEAU CALCUL";
DO: OK$ = UCASE$(INKEY$): LOOP UNTIL OK$ = "C"
GOTO Commence

END

REM****************************************************************************
CalcF:                                  ' Calcul des f(i)
    f(1) = (1 / 3) * (Y ^ 2 - (1 / Y)) / (a1 ^ 2)
    f(2) = 2 * (a1 - 1) * f(1)
    f(3) = (a1 - 1) ^ 2 * f(1)
    RETURN
REM****************************************************************************
```